Semester Thesis - Simulating qubit relaxation times to analyze limiting factors of the electromagnetic environment

Stephan Allenspach
Spring Semester 2015

Supervisor: Marek Pechal

ETH Zürich
Quantum Device Lab
Prof. Dr. A. Wallraff

August 25, 2015

Abstract

In this semester thesis a simulation program was created to simulate the limiting factors, which the electromagnetic environment has on the relaxation time T_1 of a qubit. For this the electromagnetic environment was simulated with a finite element simulator, probed artificially in a microwave signal simulator and then the relaxation time was extracted with an analysis program. This was done for different designs of the qubit to investigate how the single parameters of the qubit geometry affect the relaxation time. Also T_1 was experimentally measured for two qubits - one with and one without chargeline. The resulting relaxation times of the simulation show a weak dependency on the geometry of the qubit island and a much stronger dependency on the presence or absence of a chargeline. The simulated relaxation times are much higher than the ones obtained in the measurements, in which imperfections of fabrication and the experimental setup may play a role. This indicates a much stronger limitation of T_1 resulting from fabrication and setup than from the design. This thesis will illustrate the steps to generate such a simulation.

Acknowledgements

I would like to thank Prof. Dr. Andreas Wallraff for giving me the opportunity to conduct my semester thesis in the Quantum Device Lab. I would also like to thank Marek Pechal for introducing me to the topic, helping me with different kinds of problems, answering all sorts of questions and giving me many advises during all parts of the thesis. In advance, I would like to thank Philipp Kurpiers for his supervision in the lab and his help with the experimental setup. Additionally, I would like to thank as well Dr.Abdufarrukh Abdumalikov and Theodore Walter for helping me with questions, which came up during different steps of the thesis.

Contents

1 Introduction

The relaxation time is the time a qubit can stay in the excited state before it relaxes back into the ground state. Hence for quantum computation it is important to have a relaxation time which is sufficiently long to perform the operations needed for a protocol.
This relaxation time (called T_1) depends on different factors such as for example the qubit frequency, geometry/design of the qubit and its fabrication. Therefore, in order to build a qubit with a high T_1 one has to know how these factors affect T_1. To do that, one has to disentangle the different factors.
Since the limiting effect of the fabrication (and measurement setup) will be present for every qubit measured in an experiment, a way to separate the effects of fabrication from the design factors would be to generate a program to simulate T_1. Then by comparing the simulated to the experimentally measured T_1 (with the same design), the effect of the fabrication (plus setup) should be revealed. Also with such a program, different qubit geometries could be compared and the limiting behavior of the single parameter settings could be investigated.
The goal of this thesis was to write such a program and compare the results of different simulated geometries with each other, as well as with experimentally measured T_1 for one specific geometry.
Also the simulated T_1 could be compared to the so called "multimode model" which is a theoretical model that attempts to analytically determine T_1.
The main idea behind the whole simulation is that the qubit can be approximated as a (damped) harmonic oscillator. In frequency space, a harmonic oscillator has a Lorentzian response whose bandwidth is the inverse of the relaxation time of the harmonic oscillator. The whole simulation has the goal to first artificially measure the spectrum of the qubit by probing it with a microwave signal simulator and then extract the bandwidth of the qubit peaks to determine T_1.
This thesis consists out of three main sections. First, the different parts of the simulation will be explained in detail and the results of the simulations will be presented. Then the "multimode" model will be presented and compared to the simulated data. Finally, an overview of the performed measurements will be given and then the results of the measurement will be presented and compared to the simulation.
In the end, the results will be discussed and an outlook for potential future measurements will be given.

2 Simulation

2.1 Overview

The whole simulation consists of four different parts. First, the designs of the qubits were generated with an already existing mathematica file, which was also used to create the blueprints for the fabrication. The underlying structure of such a qubit design was then exported as a DXF file. Second, this DXF file was imported into Sonnet, a finite element simulator for the electromagnetic environment, to calculate the admittance matrix of the whole structure. Third, this Sonnet output file was used in Microwave Office as a black box and was probed artificially in reflection. Fourth, the output which was the complex amplitude of the reflected signal as a function of frequency recorded by Microwave Office, was analyzed with a mathematica program (analysis tool). This analysis program also gave feedback/commands (in the form of parameter settings for the measurement circuit) and therefore the program could loop over different values of the tuning inductance L. In the end, the output of the whole simulation was an array with frequency and bandwidth of qubit and resonator for different inductance values L, as well as the qubit-resonator-coupling g and effective capacitance C_{eff}. The whole structure of the simulation is displayed in Figure 1. In the following the different parts will be explained in more detail.

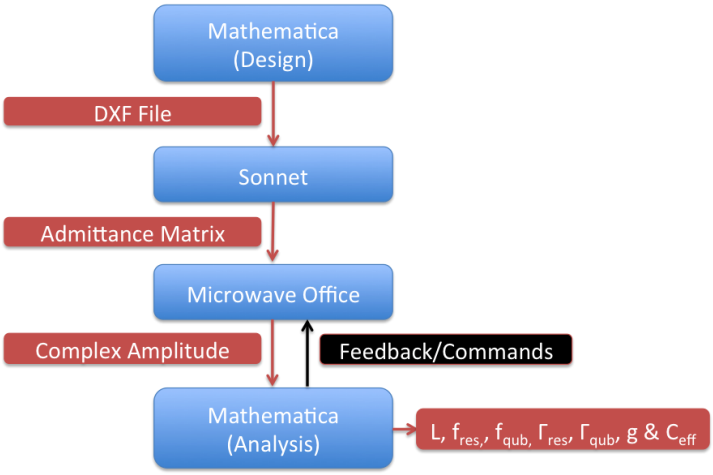

Figure 1: The different parts of the simulation and their interplay.

2.2 Design Tool

The program which builds up a qubit blueprint out of geometry settings already existed and has been used to draw the blueprints for the sample fabrication. A picture of such a blueprint is shown in Figure 2(a). The main settings to change in the design are the geometry parameters: Island separation, island width, island length and the presence or absence of the chargeline. In Figure 2(b) the three geometry parameters are depicted in an idealized qubit schematic.

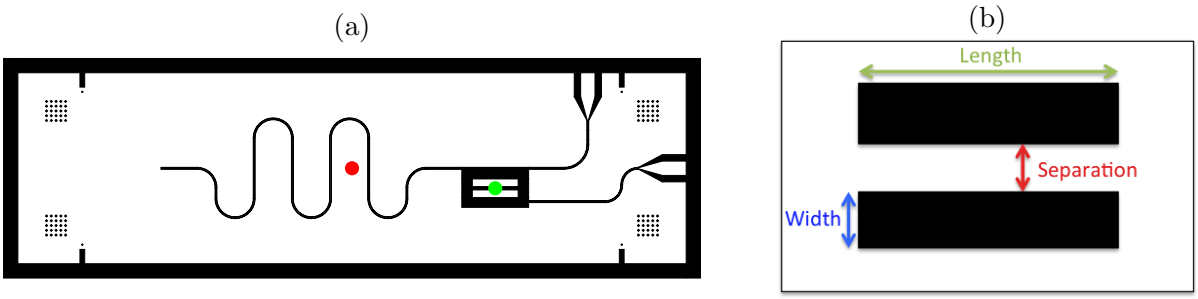

Figure 2: (a) The blueprint of a qubit with chargeline. (b) A simple qubit model with the two islands and the corresponding geometry parameters.

The geometry parameters which were changed, were the island width and the island separation. The island length wasn't changed due to time reasons. For all different parameter settings a simulation was done with and without chargeline. It is to mention that in all these blueprints the Josephson junction was not constructed since it can not be simulated with Sonnet. Also the transmission line was cut away and was then later added as a circuit element in Microwave Office. Moreover, if there was a chargeline the injector of the chargeline was cut away too. This restriction was done to reduce the size of the mesh that had to be simulated in Sonnet. On one hand, the island width was changed from 60 μm to 110 μm while the island separation was fixed to 35 μm. On the other hand, the island separation was changed from 35 μm to 100 μm while the island width was fixed to 80 μm. This was again done with and without chargeline. The extreme parameter settings are displayed in Figure 3.

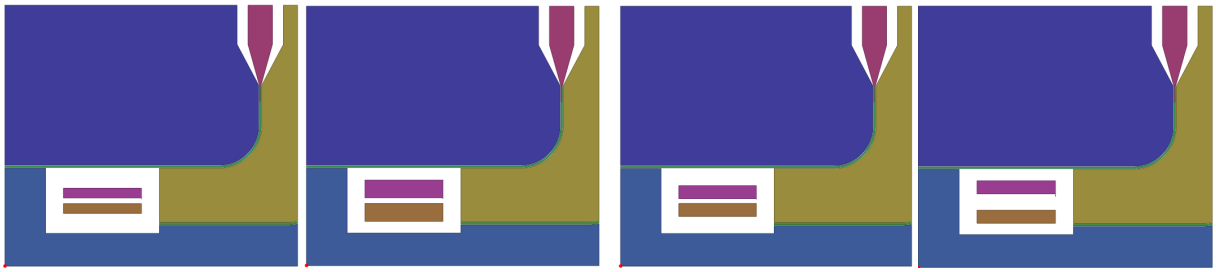

Figure 3: Different geometry parameter settings all with an island length of 480 μm. From left to right: [width=60 μm/separation=35 μm], [width=110 μm/separation=35 μm], [width=80 μm/separation=30 μm] and [width=80 μm/separation=100 μm]

2.3 Sonnet

Sonnet [6] is a licensed finite element solver for circuits which can simulate AC (in contrast to Maxwell (see 2.5) which is a DC solver and therefore cannot reliably simulate inductive effects in the circuit). The substrate was set to 500 μm sapphire and the space above the ground plate was set to 500 nm "air". The metal of the qubit was chosen to be "lossless" to simulate the effect of the niobium, which is superconducting at the qubit's working temperature. Ports were positioned at the edge of the gate line launcher, the end of the cut transmission line and if existing to the end of the chargeline (all of them touching the surface of the bounding box). To later simulate the Josephson junction, two ports were added to the two islands and both ports were set to be "co-calibrated" (and the default settings were used). The mesh grid of the number of pattern size was set to 2 microns in the x and 2 microns in the y direction. The simulated frequency range was set to 5-12 GHz for the qubit without and to 4.5-12 GHz for the qubit with chargeline. The simulations for the qubit without chargeline were almost finished when the measurements on the two qubits were performed. In these experiments frequencies below

5 GHz were performed and therefore the range was adjusted for the simulations for the qubit with chargeline (which had not been done until then). For all different designs the admittance matrix Y was calculated numerically by Sonnet for the mentioned frequency range and saved as a ".s4out" or ".s5out" file depending on the number of used ports. The problem of those output admittance matrices was that they were not purely imaginary as expected but had small nonzero real parts. In an attempt to correct this (since we assumed a lossless system) the real parts of the admittance matrices were corrected to zero (the justification of this action will be discussed in 5). A picture of one qubit design, imported into Sonnet, together with the five ports can be seen in Figure 4(a).

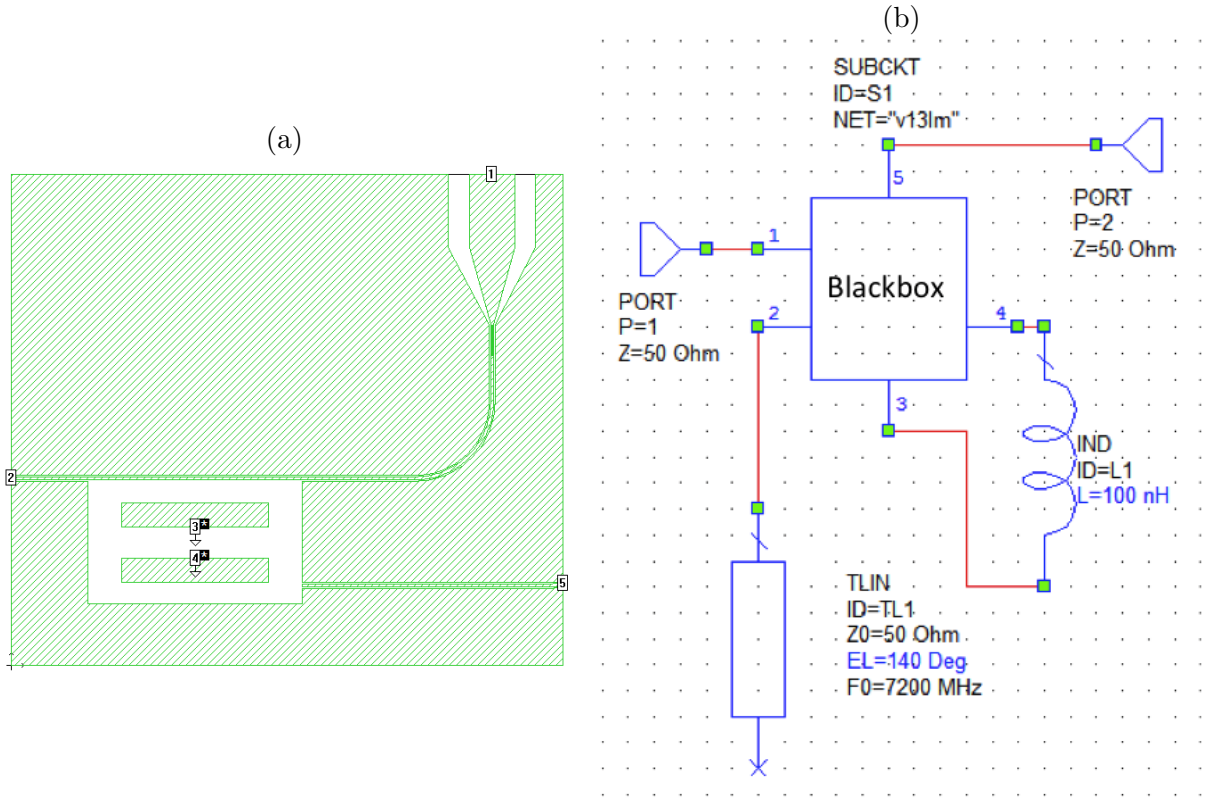

Figure 4: (a) Qubit structure in Sonnet with the three ports at the edges and the two "co-calibrated" ones next to each other at the two islands. (b) Circuit for the artificial measurement with Microwave Office.
For both figures: Port 1 corresponds to the injector, Port 2 connects blackbox and transmissionline-resonator, Port 3 & 4 are connected through the Josephson junction (inductance) and Port 5 connects blackbox and chargeline.

2.4 Microwave Office

The program Microwave Office [5] simulates microwave signals in a circuit. First the ".s4out" or ".s5out" from Sonnet were imported into Microwave Office as a black box. To this black box an inductance L was added to simulate the effects of the Josephson junction. Then artificial measurements were performed by probing the black box (/qubit) in reflection. The variation of L acts as a tuning of the qubit frequency. As mentioned, a circuit element transmission line resonator was connected to the transmission line port of the black box . The original transmission line in the blueprints was designed to give a resonator frequency of around 7.2 GHz. Hence the length of the circuit element transmission line resonator was chosen such that the resonator frequency in the simulation was also around 7.2 GHz. A signal input was connected to the port of the injector and was then used to measure in reflection. For this, a signal with a certain

frequency ν was sent from the Microwave Office port (called "PORT P=1" in Figure 4) to port 1 of the black box and the complex amplitude (real and imaginary part) of the back-reflected signal was recorded. This was done automatically by Microwave Office for every frequency in a chosen frequency range (with a maximal number of 10001 steps possible). The output was a table (.txt file) with three columns: frequency, real part and imaginary part of the amplitude. If there was a chargeline, then also one pin was added to the port of the chargeline without using it explicitly. This was done to capture the effect of dissipation into the $50\,\Omega$ chargeline. An overview of the circuit in Microwave Office for the artificial reflection measurements is visible in Figure 4(b).

2.5 Maxwell

As mentioned, it is also possible to use another finite element solver to simulate the on chip environment. For example one could use Maxwell[4] instead of Sonnet. Maxwell can also import the DXF file (output of the design tool), simulate the electromagnetic environment and then exports the capacitance matrix (instead of the admittance matrix when using Sonnet). However, Maxwell is a DC solver which means that inductive effects can not be simulated. But those effects are neglectable when the size of the simulated region is much smaller than the wavelength (as in our case). The overview of the whole structure with Maxwell instead of Sonnet is visible in Figure 5.

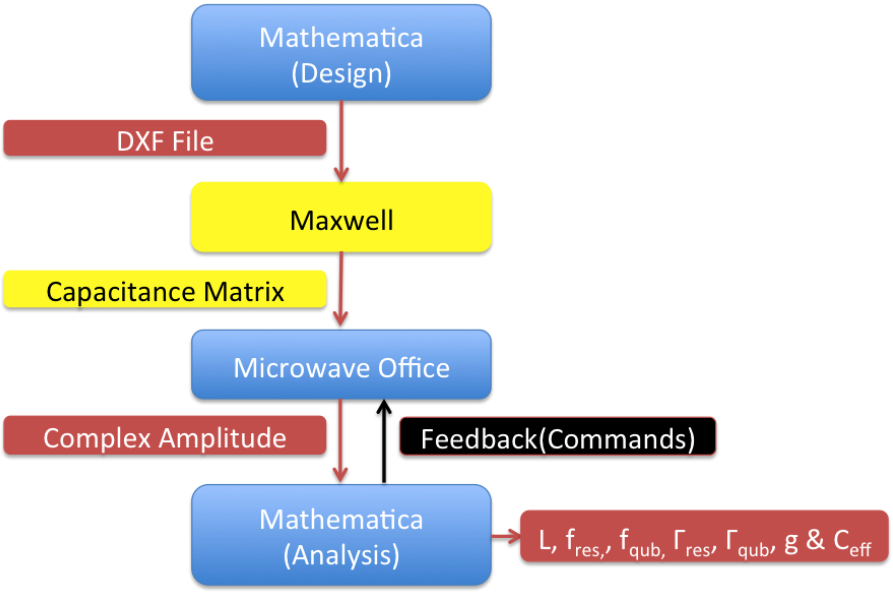

Figure 5: The overview of the whole structure when Maxwell is used instead of Sonnet.

The entries of this capacitance matrix include all capacities between the different elements themselves and between the different elements and ground. This capacitance matrix can not simply be imported into Microwave Office as in the case for the admittance matrix exported from Sonnet. Hence a capacitance network had to be built in Microwave Office and all the values for the capacitances had to be inserted manually. A picture of such a capacitance network is displayed in Figure 6. The qubit is then constructed as LC-circuit in Microwave Office. The capacitance C of this LC-circuit is the capacitance between the islands calculated by Maxwell, while the inductance L is used to tune the qubit frequency (as in the case of Sonnet).

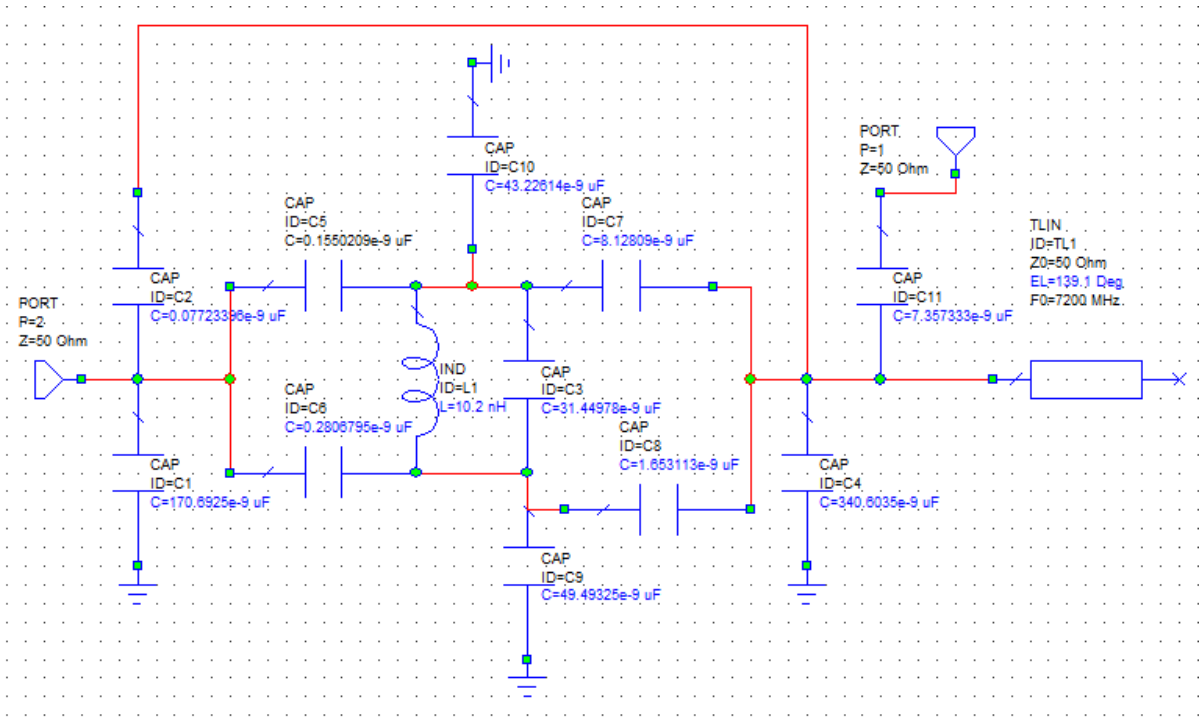

Figure 6: The capacitance network (constructed in Microwave Office) which corresponds to the entries of the capacitance matrix. The qubit is the LC-circuit in the middle which is coupled capacitively to the same elements as for the "Sonnet-blackbox".

2.6 Analysis Tool

The simulated data from Microwave Office were analyzed in a Mathematica file. Also this Mathematica file adjusted the Microwave Office settings such that a loop over different values of L ($\approx$ different qubit frequency tunings) was possible. Since no way was found to easily control Microwave Office directly from Mathematica, an in-between program was used. For this purpose a Python script was written, which can control Microwave Office (see the webpage listed as [7] for the module to control MWO from python). And from Mathematica such a Python script is easily controllable using Windows command line. This combination then allowed us to control Microwave Office from Mathematica. The frequency range, frequency step size and the inductance L used in the Microwave Office setup were sent from the Mathematica analysis file to Microwave Office. The scheme for this procedure is depicted in Figure 7(a).

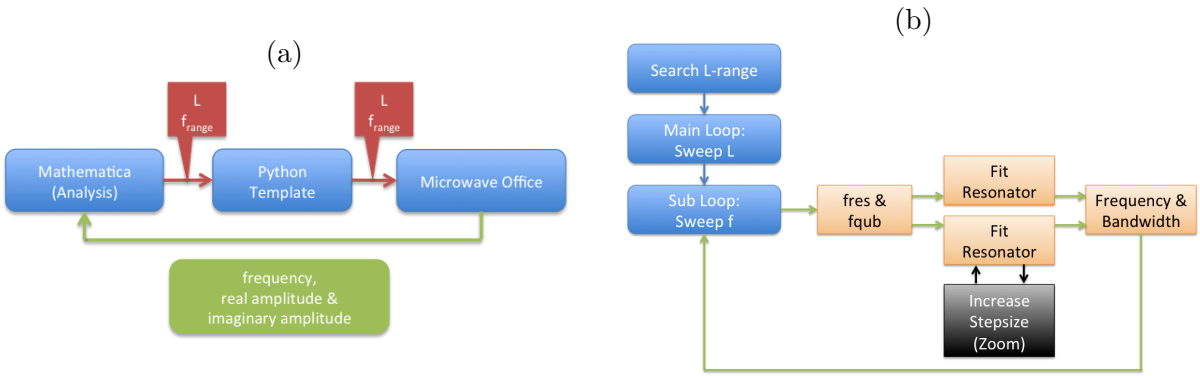

Figure 7: (a) Schematic drawing of the interface between the Mathematica analysis tool and Microwave Office. (b) An overview of the different loops and tasks within the analysis tool.

2.6.1 Procedure

In the following subsections, the steps performed by the Mathematica script will be explained in detail.
The program swept over different inductances L, which correspond to different qubit frequencies (since the inductance is a placeholder for the Josephson junction and therefore the qubit frequency can be tuned by varying L). The real and imaginary part of the back reflected signal amplitude have the shape of a Lorentzian for the qubit and resonator. So for each L, the position and the width of the frequency peaks of the resonator and qubit were determined by simultaneously fitting the real and imaginary parts with a complex Lorentzian. This included, in addition to the sweeping of L, also a change of the probed frequency range and step size to gather better data for the fits (see 2.6.3). Then T_1 could be calculated because it is given by the inverse of the qubit peak width. An overview of the different tasks is shown in Figure 7(b).

2.6.2 Search L-range

As mentioned, a variation of L corresponds to the tuning of the qubit frequency. Hence in the spectrum the qubit frequency will be shifted for different values of L. This behaviour is displayed in Figure 8.

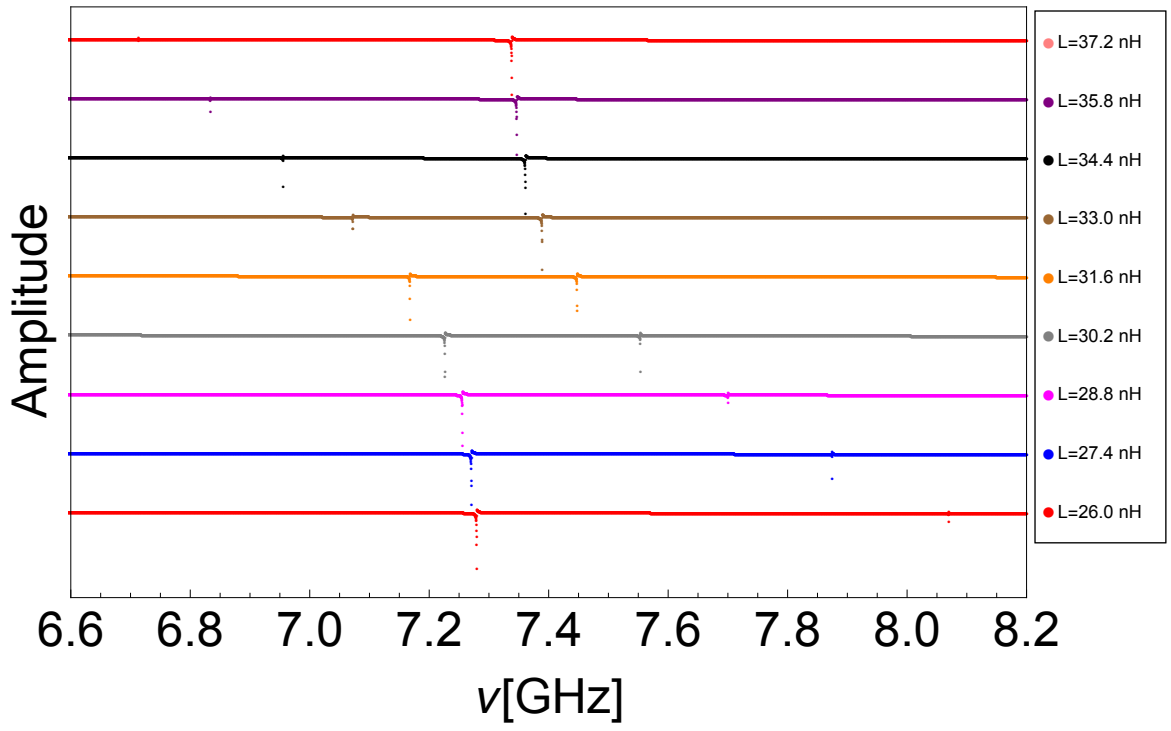

Figure 8: The spectrum is plotted as a function of the probing frequency for different values of L. It is observable how the qubit peak shifts significantly when changing the value of L while the resonator peak is just shifted a little. In the on-resonant-region, the qubit and resonator peak can not be distinguished anymore and at a certain value of L ($\sim$31 nH), the qubit and resonator peak exchange places.

Since just a certain range of frequencies were simulated with Sonnet (5 GHz to 12 GHz for qubits without chargline and 4.5 GHz to 12 GHz for qubits with chargeline), just a certain range of values of L lead to qubit frequencies which lied in the mentioned frequency regions. So the first task was to find this range by increasing L (from a value where no qubit peak was visible)

until the qubit peak was suddenly visible (L_{min}) and then increasing it further until the qubit peak wasn't visible any longer (L_{max}).
Then the program looped over the values of L lying in this range ($L \in [L_{min}, L_{max}]$). This was done with an adaptive stepsize. What does this mean? For a fixed L, the bandwidth and position of the qubit and resonator peaks were determined. The stepsize was set, depending on those four values such that more steps were taken in the on-resonant-region than in the off-resonant-region (this was done to get a better fit of the qubit-resonator-coupling g).

2.6.3 Main Loop: Sweep L

For a fixed L there was one spectrum output from Microwave Office for the whole frequency range with a resonator and a qubit peak visible (since just values of L where this is valid were probed). From this spectrum the position of the qubit and resonator peak were determined. If necessary the program could "zoom in" to fit the resonator and qubit peak better. This "zoom" can be understood as a command from the Analysis Tool to Microwave Office to give an output of the spectrum around the resonator or qubit frequency with a range such that a nice peak (resonator or qubit) was visible. And of course without the other peak and with a stepsize such that a good fit of the single Lorentzian was possible.

2.6.4 Sub Loop: Sweep f

For the resonator the peak was very broad, hence usually one zoom was enough to fit the resonator peak with a Lorentzian (and extract the bandwidth and exact position out of the fit).
For the qubit, which has a very narrow peak in the off-resonant-region, the program zoomed in once with the same zoom settings (frequency step size etc.) as for the resonator and tried to fit the data. If the program couldn't fit the data properly, it gave the command to zoom in again. This was done until the qubit peak could be fitted or until seven zooms were performed. The restriction to a maximal number of zooms was needed to suppress infinite loop generation, which could occur when the peaks were to narrow or when one of the fits failed, resulting in incorrect zooming.
After a good fit was obtained, the bandwidth and exact frequency position of the qubit peak were extracted. An example fit of the data with a Lorentzian is visible in Figure 9

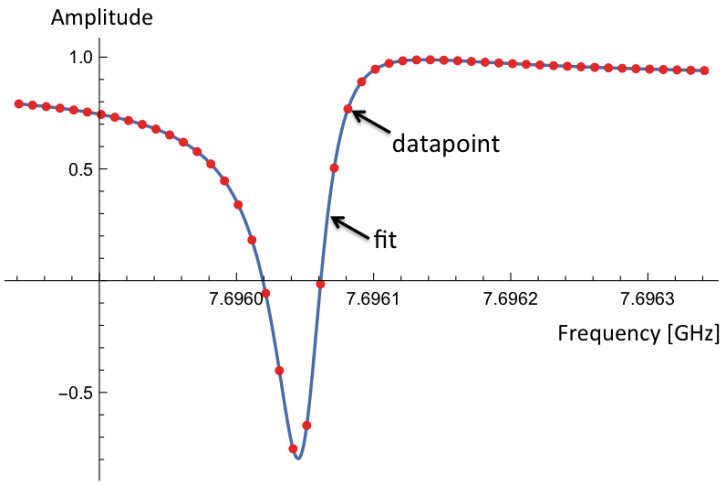

Figure 9: The (zoomed) data from Microwave Office (red points) was fitted with a Lorentzian (blue line).

In the end, the output of this looping procedure was an array for different values of L and corresponding arrays for the bandwidths and frequencies of the qubit and the resonator.

2.6.5 Resulting frequencies and bandwidths

Since the qubit frequency ν_{qubit}, the resonator frequency ν_{res}, the qubit bandwidth Γ_{qubit} and resonator bandwidth Γ_{res} are connected through L, they can be plotted as functions of each other. For example ν_{qubit} and ν_{res} can be plotted both as a function of L. This was done in Figure 10, where the avoided crossing in the on-resonant-region is visible.

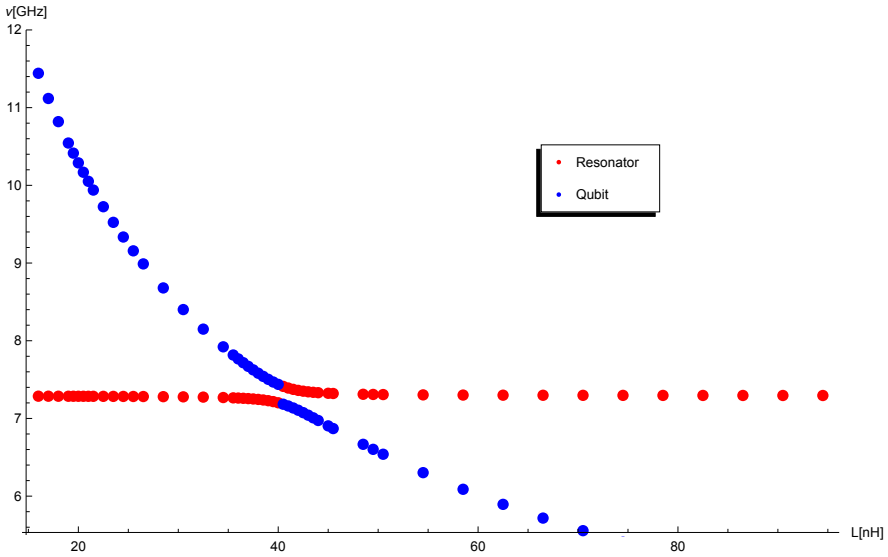

Figure 10: The frequencies of the qubit and resonator are plotted as a function of L (tuning of the qubit). Also an avoided crossing is visible in the on-resonant-region.

Also Γ_{qubit} and Γ_{qubit} can be plotted in dependency of L. This was done in Figure 11.

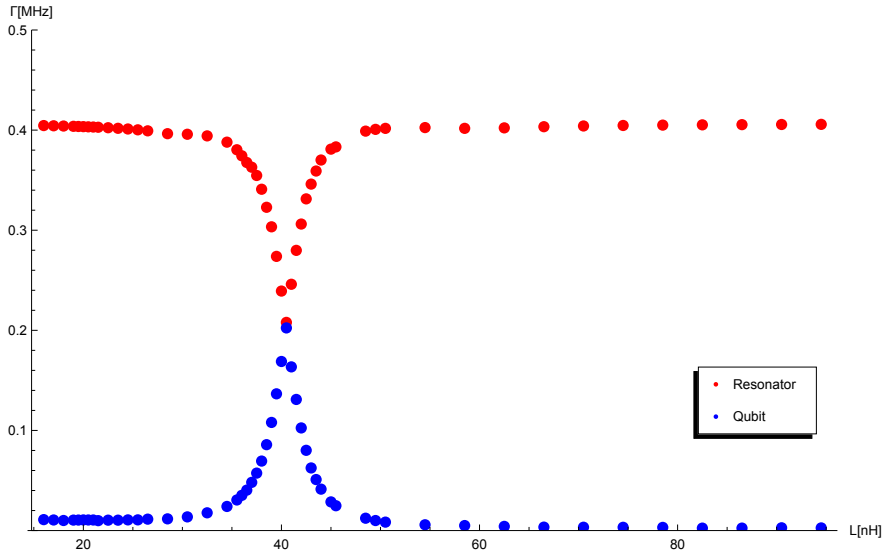

Figure 11: The bandwidths of the qubit and resonator are plotted as a function of L (tuning of the qubit).

2.6.6 Extracting g and C_{eff} with a fit

To extract the qubit-resonator-coupling g one has to look at the distance between the qubit and the resonator frequency $\Delta = |\nu_{qubit} - \nu_{resonator}|$. With this quantity one can extract the qubit-resonator-coupling g by fitting the data Δ as a function of L with the fit function

$$\Delta(L) = \sqrt{\alpha\Big(\frac{1}{\sqrt{L}} - \frac{1}{\sqrt{L_0}}\Big)^2 + (2\tilde{g})^2} \tag{1}$$

with L_0 as the inductance where Δ is minimal, $\tilde{g} = g/2\pi$ and α an unknown proportionality constant. A plot of the fitted data is shown in Figure 12.

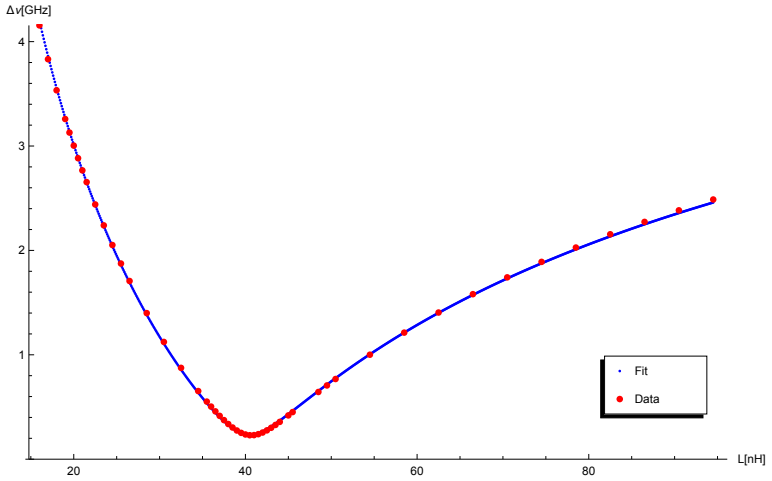

Figure 12: Fit of the data Δ vs L, which was fitted with equation (1) to extract g.

Another quantity which can be extracted, is the effective capacitance of the qubit C_{eff}. This can be done by fitting the data ν_{qubit} as a function L with the fit function

$$\nu_{qubit}(L) = \frac{1}{2\pi\sqrt{LC_{eff}}} \tag{2}$$

An example of such a fit of the data is displayed in Figure 13. Equations 1 and 2 are derived in Appendix 7.7.2.

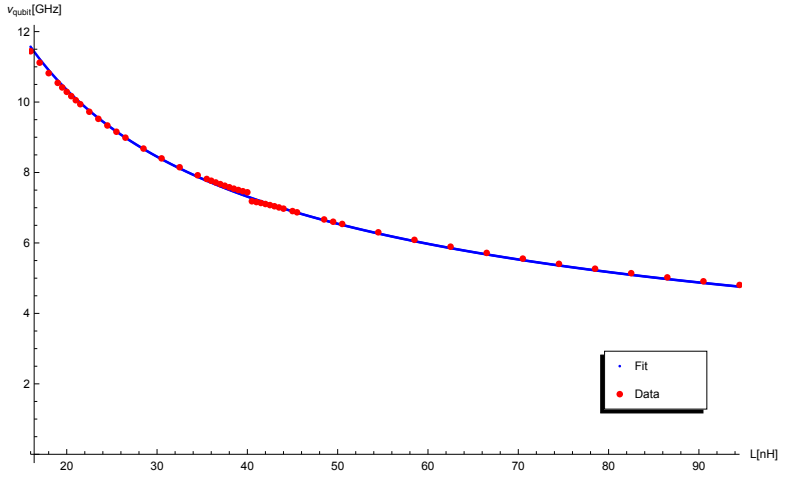

Figure 13: A fit of the data ν_{qubit} vs L, which was fitted with equation (2) to extract C_{eff}.

2.7 Results of the simulation

2.7.1 Sweep of the island width

Simulations were performed for different values of the island width (see Fig.2(b)), while the island separation was fixed at 35 μm and the island length was fixed at 480 μm. The different values of the island width were:
60 μm, 70 μm, 80 μm, 90 μm, 100 μm and 110 μm.
For each value of the width, the qubit was simulated with and without chargeline. The resulting values for the qubit-resonator-coupling g are shown in Figure 14 and for the effective capacitance C_{eff} in Figure 15.

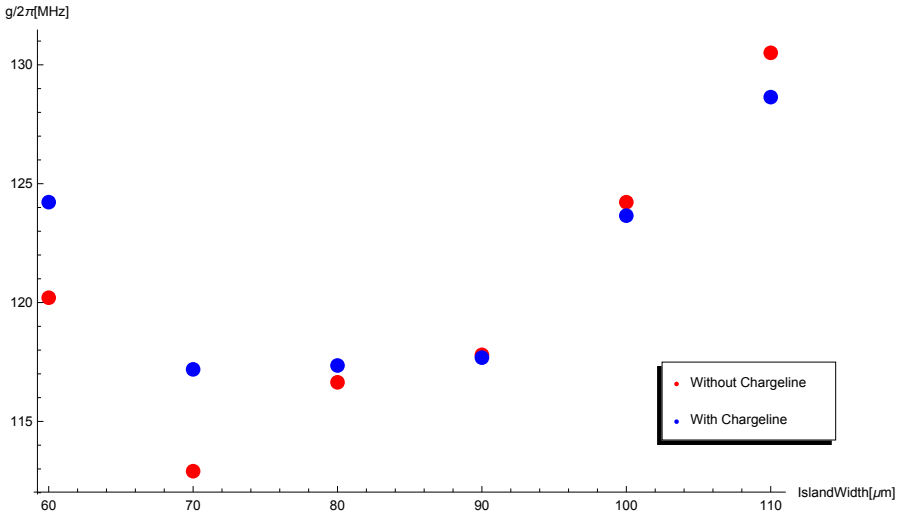

Figure 14: The qubit-resonator-coupling g is plotted as a function of the island width for a qubit with and without chargeline.

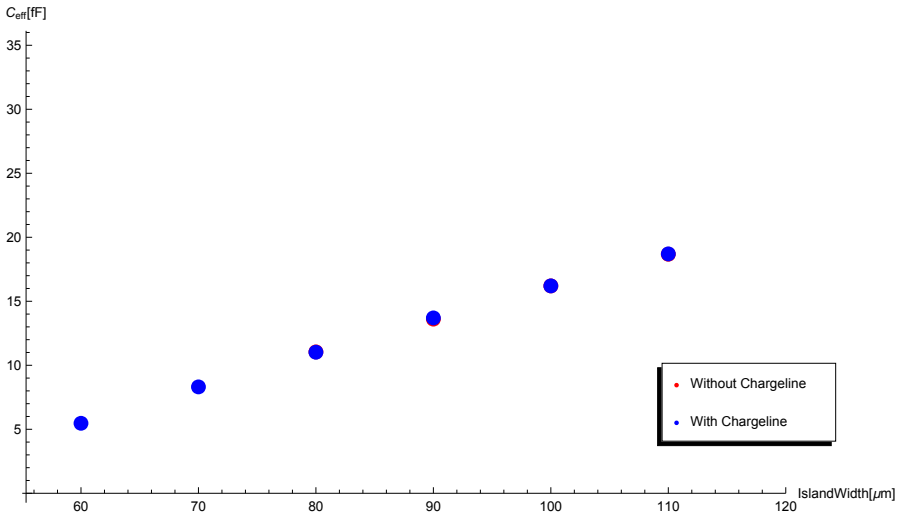

Figure 15: The effective capacitance C_{eff} is plotted as a function of the island width for a qubit with and without chargeline.
Note: The data points for the two cases are overlapping.

As mentioned, T_1 is the inverse of the qubit bandwidth Γ_{qubit}. The resulting values for T_1 in dependency of the qubit frequency ν_{qubit} are plotted logarithmically for the qubit with chargeline in Figure 16 and for the qubit without charge line in Figure 17. For clarity, only sweeps for a few selected values of the width are displayed in those two plots.

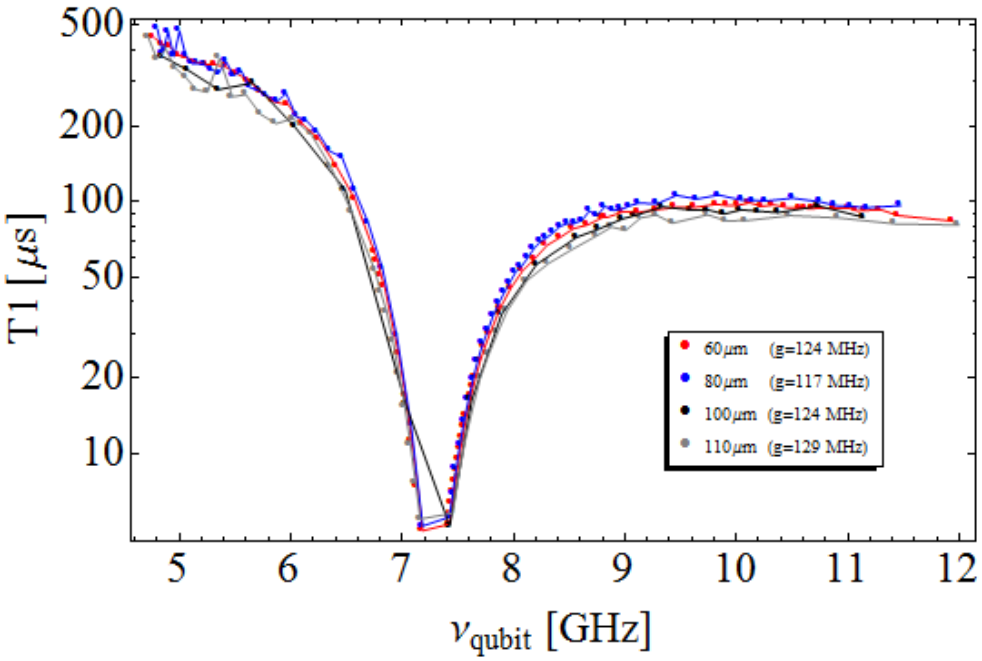

Figure 16: The relaxation time T_1 is plotted logarithmically as a function of the qubit frequency ν_{qubit} for a qubit **with** chargeline. The different colors correspond to different values of the island width.

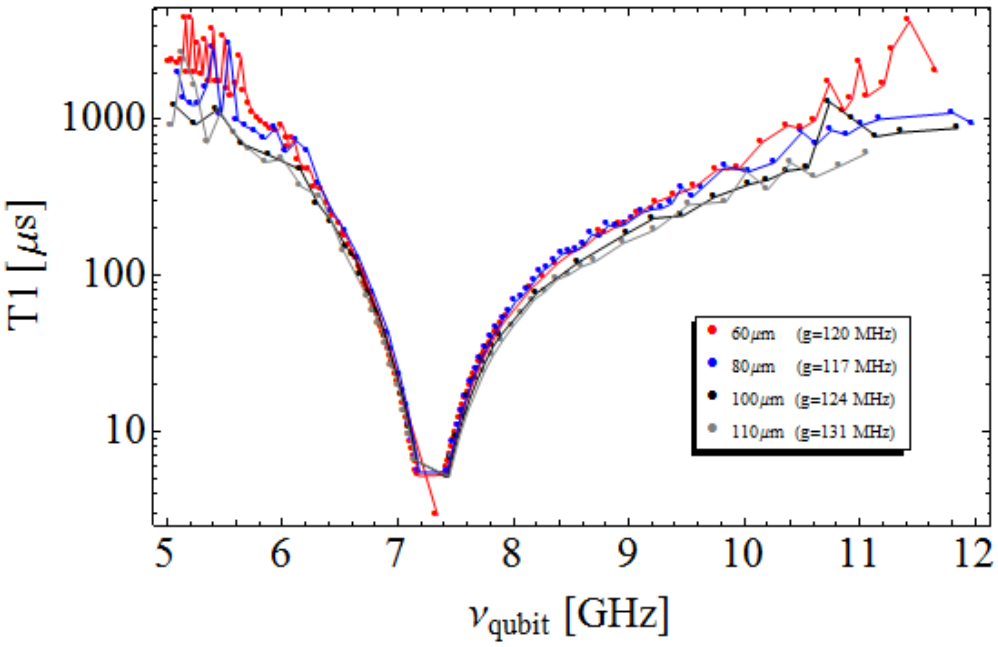

Figure 17: The relaxation time T_1 is plotted logarithmically as a function of the qubit frequency ν_{qubit} for a qubit **without** chargeline. The different colors correspond to different values of the island width.

2.7.2 Sweep of the island separation

Similarly, simulations were made for different values of the island separation while the island width was fixed at 80 μm and the island length was fixed at 480 μm. The different values of the island width were:
30 μm, 35 μm, 40 μm, 45 μm, 50 μm, 55 μm, 60 μm, 70 μm, 80 μm, 90 μm and 100 μm.
For each value of the separation, the qubit was simulated with and without chargeline. The resulting values for the qubit-resonator-coupling g are shown in Figure 18 and the resulting values for the effective capacitance C_{eff} are shown in Figure 19 for a qubit with and a qubit without chargeline.

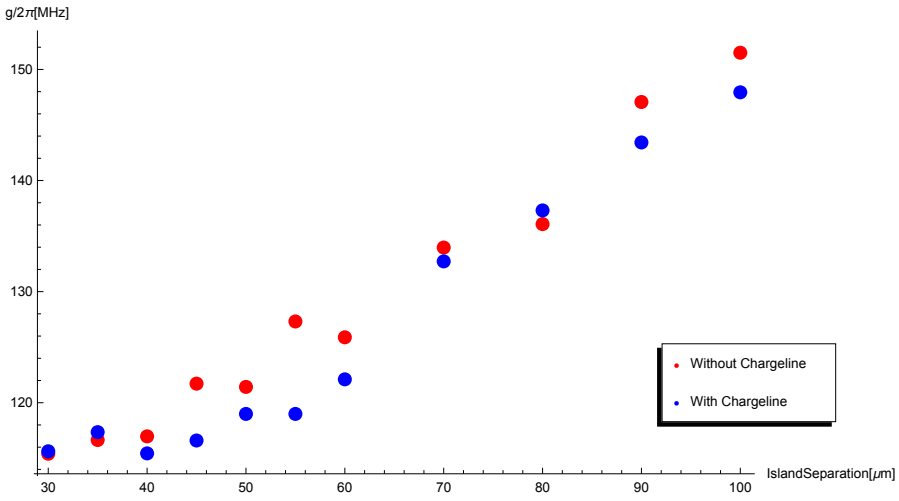

Figure 18: The qubit-resonator-coupling g is plotted in dependency of the island separation for a qubit with and without chargeline.

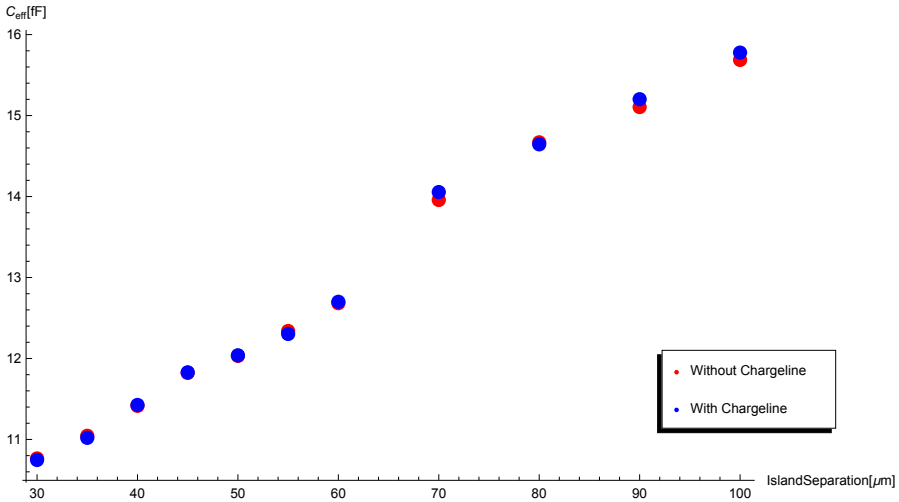

Figure 19: The effective capacitance C_{eff} is plotted in dependency of the island separation for a qubit with and without chargeline.

The resulting values for T_1 in dependency of the qubit frequency ν_{qubit} are plotted logarithmically for the qubit with chargeline in Figure 20 and for the qubit without chargeline in Figure 21. Also in those two plots not all sweep spots are displayed due to the same reason as for the figures of the sweep of the width.

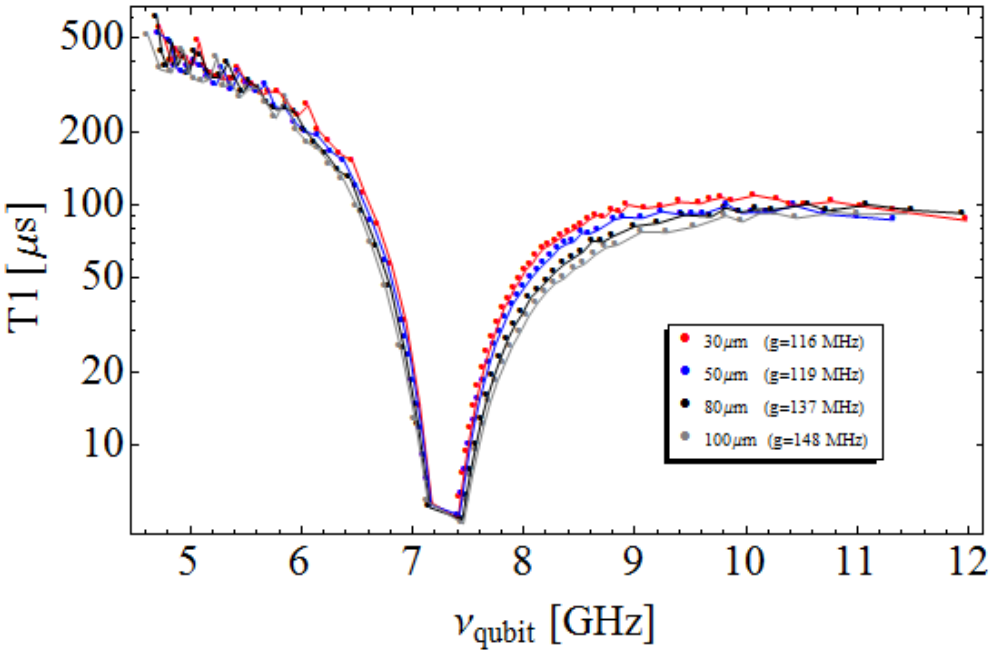

Figure 20: The relaxation time T_1 is plotted logarithmically as a function of the qubit frequency ν_{qubit} for a qubit with chargeline. The different colors correspond to different values of the island separation.

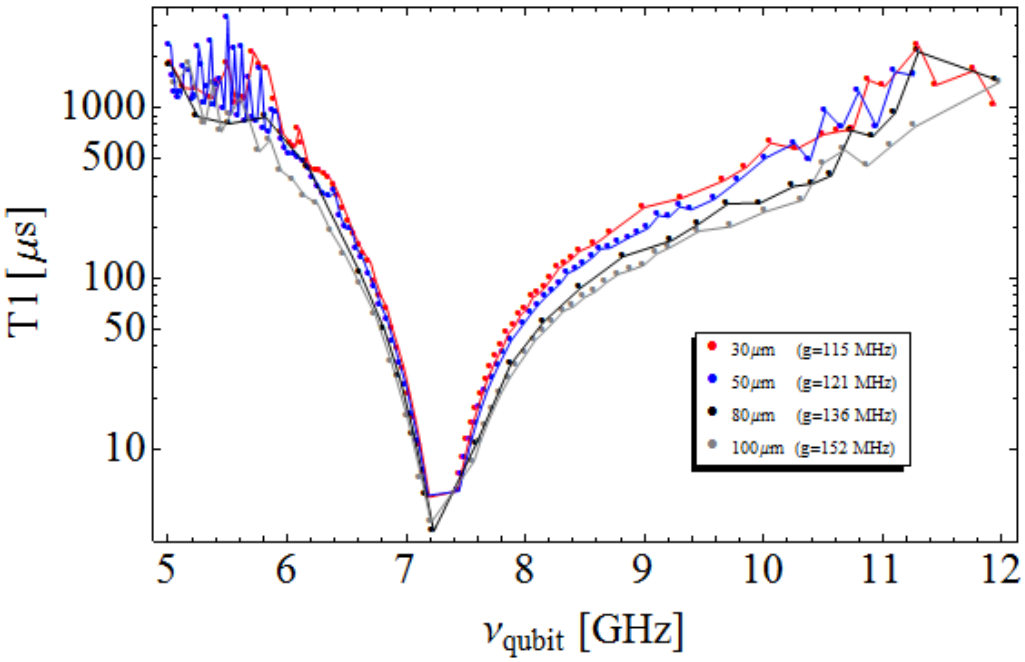

Figure 21: The relaxation time T_1 is plotted logarithmically as a function of the qubit frequency ν_{qubit} for a qubit without chargeline. The different colors correspond to different values of the island separation.

2.7.3 Comparing T_1 with and without chargeline

Another interesting thing is to compare the resulting value for T_1 for a qubit with and without charge line. In Figure 22, T_1 is plotted logarithmically as a function of the qubit frequency ν_{qubit}. For this comparison the chosen geometry parameters were: Island width 80 μm, island separation 35 μm and island length 480 μm for both qubits.

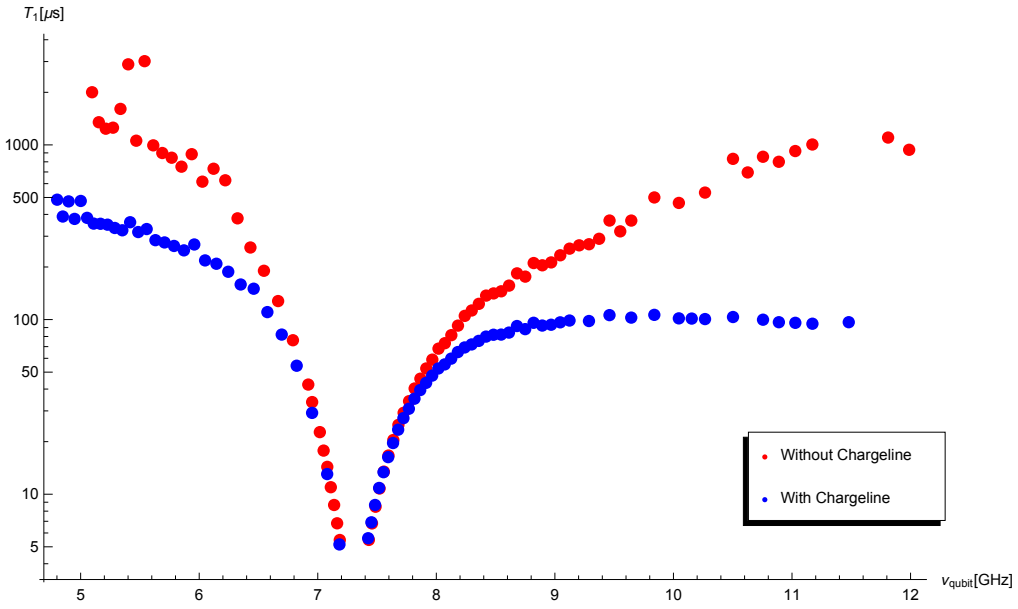

Figure 22: T_1 as a function of the qubit frequency ν_{qubit} to compare a qubit with the same geometry but with and without chargeline.

2.7.4 Interpretation

It is visible that the change of the island width or the island separation has an effect on T_1 or g, but the effect is not very strong.
The values for C_{eff} are small compared to what one would have expected. To be more concrete, for E_C/h =300 MHz a C_{eff} ~70 fF would be the expected effective capacitance.
Moreover, for very high T_1 the data starts to be very noisy. This is most likely a numerical effect, because the inverse of a very small quantity is taken, which can lead to numerical errors.
In the plot of the qubit-resonator-coupling g as a function of qubit width (see Fig.18), a minimum for both qubits (with and without chargeline) is visible. This minimum is unexpected and might be a result of a numerical error for the simulation of the island width = 60 nH, since no such minima are visible for C_{eff}.
By looking at the comparison of the simulation for a qubit with and without chargeline, it is visible that the resulting T_1 start to differ very much for frequencies in the off-resonant-region. This difference is much bigger than the differences in the geometry parameter sweeps. So in the simulation the chargeline has a much bigger limiting effect on T_1 than the geometry parameter settings have.

3 Model

Another goal was to check if the so called "multimode model" matches with the simulated data. But why is a model important? It would be nice to have an analytical model which describes the behaviour of T_1 for different qubit frequencies. First, this analytical model would be a much faster way to estimate if a geometry is "good" or "bad" since the simulation takes its time to produce results. Second, an analytical model matching the data would give us a better intuition for the behavior of the system compared to just simply simulating the system numerically. A simple model which includes just a single mode (Purcell decay model) doesn't describe the behavior of the qubit very accurately [2]. To change that, the multimode model comes into the game, where different modes are implemented. This model is derived in Appendix 7.3 and describes qubits without chargeline. The relaxation rate of this model is given by

$$\Gamma = \frac{2g^2\pi\omega}{\omega_0^2} \frac{\left(\omega C Z_0\right)^2 \cos^2(\phi)}{\sin^2(\phi) + \omega C Z_0 \sin(2\phi) + \left(\omega C Z_0\right)^2} \tag{3}$$

with ϕ the phase shift accumulated by a signal at frequency ω propagating over one length of the transmission line resonator, g the qubit-resonator-coupling and C the coupling capacitance between the resonator and the output line of characteristic impedance Z_0 (see Appendix 7.3). This model contains different modes and therefore interference effects. In the near-resonant-region, energy transmission through the resonator leads to dissipation and creates a dip in T_1. In the off-resonant-region, the energy transmission through the resonator is suppressed and destructive interference between different modes (Purcell protection) leads to a pole in T_1.

3.1 Comparing Simulation and Model

In Figure 23 the output of the simulation for the qubit with 480 μm island length, 60 μm island width and 35 μm island separation (and without chargeline) is plotted together with the multimode model function. It should be noted that only the proportionality constant between frequency and the phase ϕ, which sets the frequency of the resonator, was fitted. The coupling g was extracted from the frequency separation of the avoided crossing.

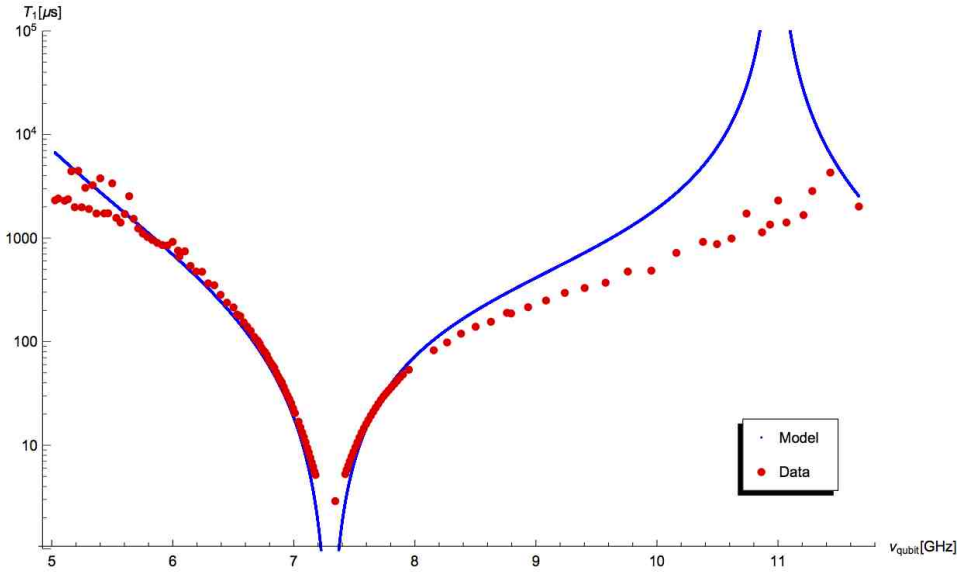

Figure 23: The simulated output data of T_1 (red dots) are plotted logarithmically together with the "multimode model" values of T_1 (blue line) from 5 GHz to 12 GHz.

As a remark $min(\Gamma_{resonator})$ was taken too from the simulation (for an explanation how and why, see Appendix 7.3). The mentioned behavior of the model is visible in Figure 23.

The data of the model and the simulated data match very well in the on-resonant-region and start to differ much in the off-resonant-region. The data do not show any sign of having a pole in the region where the model has one.
To be sure that the data has a second dip in T_1 at the double resonator frequency (multimode behaviour) and doesn't just increase for higher frequencies a simulation for the range 5 GHz to 20 GHz was performed for the same design (island length 480 μm, island width 60 μm and island separation 35 μm and no chargeline) and is displayed in Figure 24 where the expected second dip is visible at $\sim$ 14 GHz.

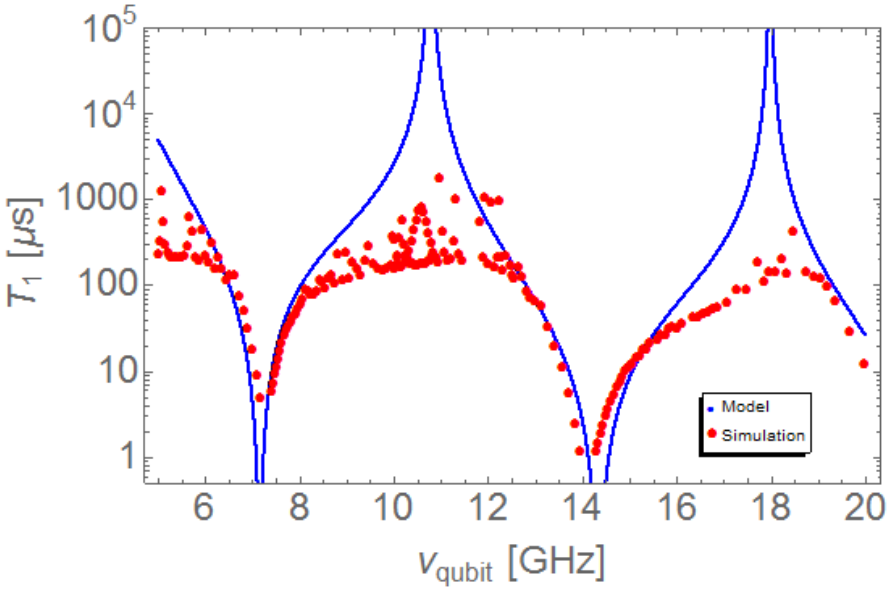

Figure 24: The simulated output data of T_1 (red dots) are plotted logarithmically together with the "multimode model" values of T_1 (blue line) from 5 GHz to 20 GHz.

This time much more points were simulated in the region in between the two dips and strong numerical fluctuations are visible in the off-resonant-region in between the two dips too.

3.2 Interpretation

The simulated data seem to be somehow limited in magnitude when compared with the model. So in an attempt to find the reason for the difference, a constant offset was added to the bandwidth of equation (3) $\Gamma \to \Gamma + \delta$ with a constant offset $\delta > 0$. This results in a reduced relaxation time $T_1^{off} = 1/(\Gamma + \delta) < 1/\Gamma = T_1$. In Figure 25 the simulated data from above is plotted again with the "multimode model" together with the "offset model", in which a constant offset of δ=250 Hz was added to equation 3 and then the inverse was taken.

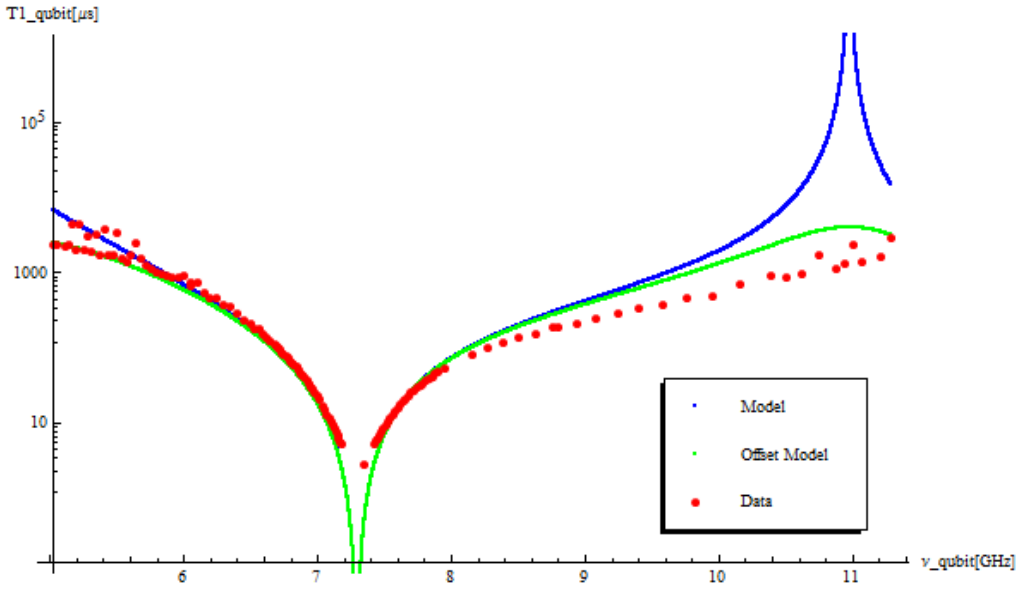

Figure 25: Simulated output data for T_1 (red dots), the "multimode model" (blue line) and the "offset model" (green line).

It is to mention that the constant offset was chosen (and not fitted) just to show the effect such an offset would have and can not be taken as exact. Also the offset model doesn't match the behavior of the simulated data completely but better than the normal model without offset. It can be interpreted as a step into the right direction but not as the full explanation for the difference between the model and the simulated data. So the interesting question is what causes the observed losses since all the metal and dielectrics were set lossless in Sonnet. This problem will be taken up again in the final discussion in 5.

4 Measurement

Two qubits with the same geometry but one with and one without chargeline were fabricated to perform measurements in the lab. The qubits had an island width of 80 μm, an island separation of 35 μm and an island length of 480 μm. A photo of the qubit without chargeline is visible in Figure 26(a). Both qubits were put on the same sample holder with separate coils (so they could be tuned separately). The sample was put into a cryostat and was probed in reflection. The used sampleholder for the two qubits is visible in Figure 26(b).

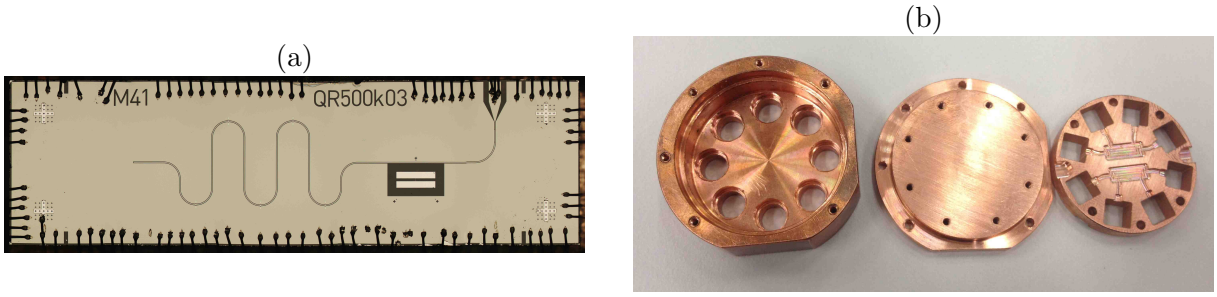

Figure 26: (a) A photo of the qubit without chargeline. (b) The used sampleholder parts.

The dephasing time T_2^* and the relaxation time T_1 was measured for different qubit frequencies (different tunings of the magnetic field) for both qubits. The measured qubit frequencies are plotted as a function of the applied "coil-voltage" (proportional to the magnetic flux through the qubit's SQUID loops) for both qubits in Figure 27.

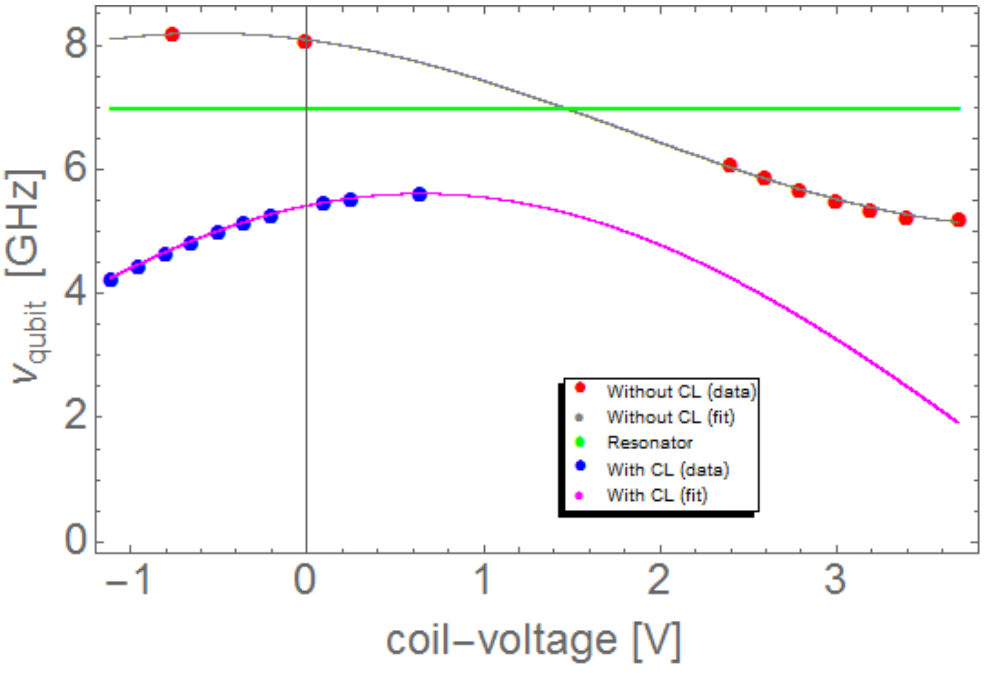

Figure 27: The different qubit frequencies are plotted in dependency of the applied voltage through the coils for both qubits. Also the position of the resonator frequency is marked with a solid green line. The other two solid lines correspond to cosinusoidal fits of the qubit frequency $\nu_{qubit} \propto \sqrt{\cos(\phi/2)}$ with ϕ the phase corresponding to $\phi = \frac{2\pi\Phi}{\Phi_0}$ with the magnetic flux Φ through the qubit and Φ_0 the magnetic flux quantum.

Even though both qubits had equal blueprints (just with and without chargeline) and were designed to have the same maximum frequency $\nu_{qubit}^{\max}$ (the so-called sweetspot), they turned out

to be different in the measurements. Also the qubit without chargeline had a second (lower), unexpected sweetspot ($\nu_{qubit}^{minimal}$ in this case), which wasn't designed either.

4.1 Measurement Methods

Three types of measurements were performed for each tuning to estimate the relaxation time T_1 and dephasing time T_2^*. First, a Rabi measurement was done to determine the amplitude for a π- and a $\frac{\pi}{2}$-pulse. In a Rabi measurement the population is plotted as a function of the amplitude of the signal. The data can be fitted with a trigonometric function (Rabi oscillations), which gives the amplitudes for a π- and a $\frac{\pi}{2}$-pulse. The plot for such a Rabi Measurement (data and fit) is shown in Figure 28(a).
Second, a Ramsey Measurement was performed to determine the dephasing time T_2^*. For this a $\frac{\pi}{2}$-pulse is applied to kick the state vector from the ground state to the superposition state (equator of the Bloch sphere). After a certain time period t, a second $\frac{\pi}{2}$-pulse is applied to kick the state vector from the equator of the Bloch sphere to the z axis and subsequently the state is measured. This is done for different times t. The resulting data can be fitted with an oscillating exponential decay and the decay constant corresponds to the inverse of the dephasing time T_2^*. The plot of such a Ramsey Measurement (data and fit) is displayed in Figure 28(b).
Third, a measurement of the relaxation time T_1 was performed in the following way: A π-pulse is applied to the ground state to kick the state up into the excited state and then after a certain time t the state is measured. This is repeated for different times t. The resulting data can then be fitted with an exponential decay, whose decay constant is the inverse of the relaxation time T_1. The corresponding plot (data and fit) is shown in Figure 28(c).

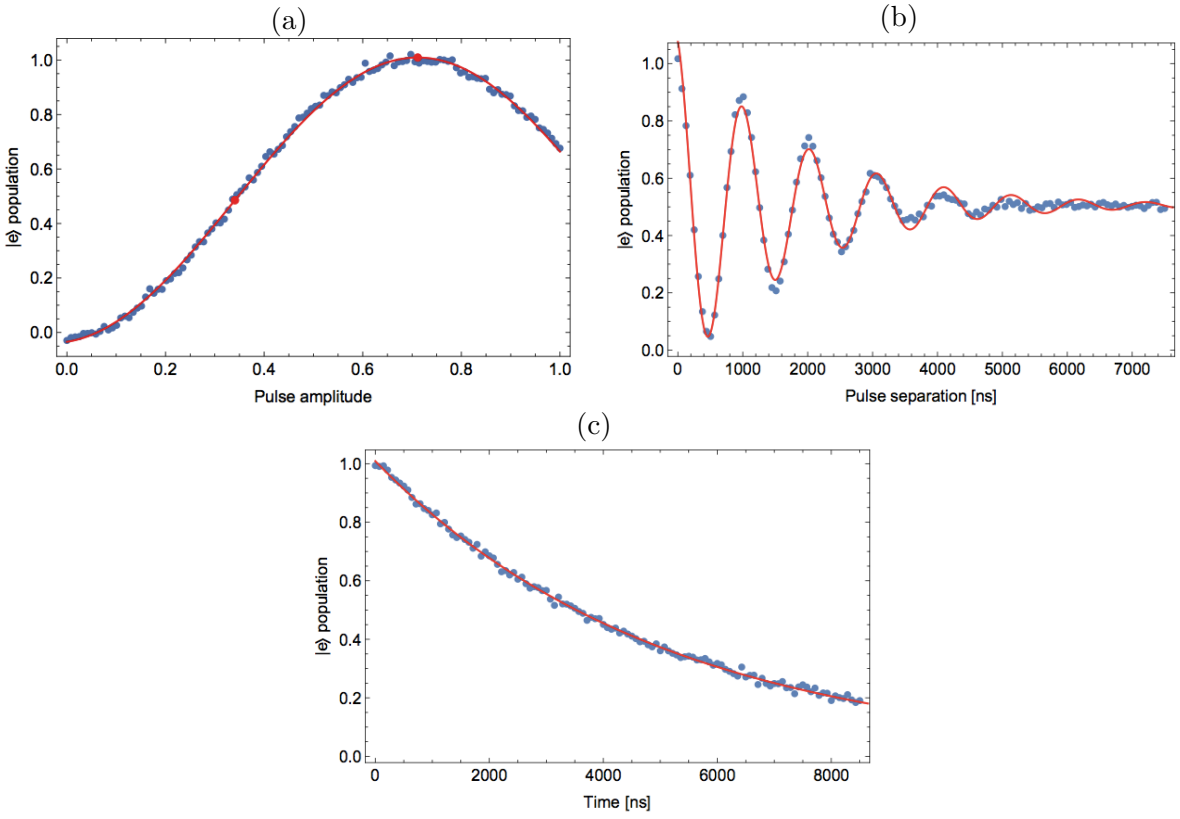

Figure 28: The data and corresponding fits for a Rabi Measurement (a), a Ramsey Measurement (b) and a T_1-Time-Measurement (c).

All measurements were performed more than once for the same settings. As final value the statistical mean and for the error the statistical standard deviation were taken.

4.2 Measurement Results

The resulting T_2^* and T_1 for the qubit with chargeline and without chargeline are plotted logarithmically together as a function of the qubit frequency in the Figures 29 and 30.

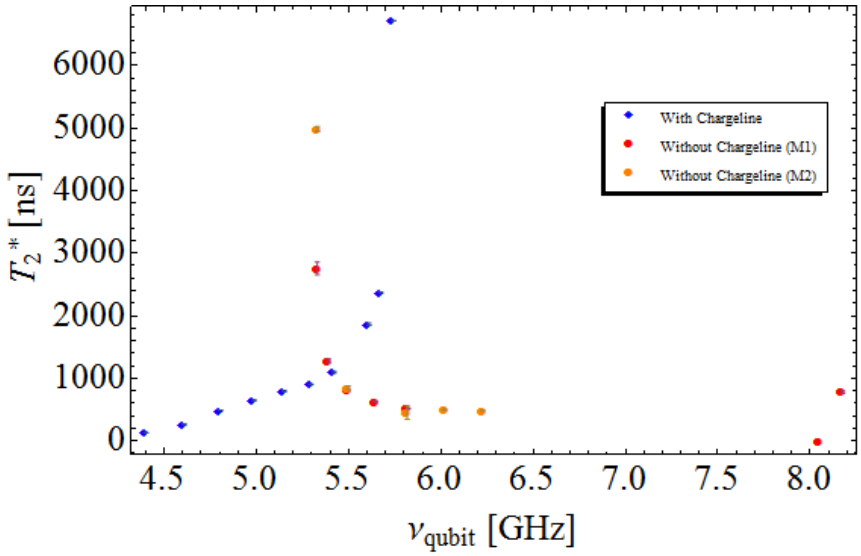

Figure 29: The measured dephasing times T_2^* are displayed for different qubit frequencies for both qubits.

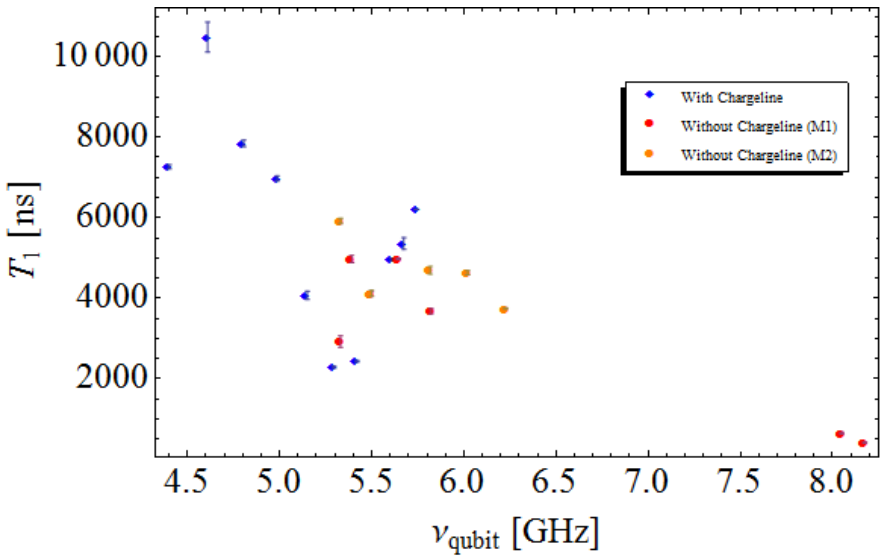

Figure 30: The measured relaxation times T_1 are displayed for different qubit frequencies for both qubits.

4.2.1 Remarks on the qubit with chargeline

In the plot of the relaxation times T_1 an unexpected dip is visible at around 5.3 GHz. This dip could correspond to a fundamental mode of a standing wave in the chargeline. But due to the

restriction of the qubit frequency range, it wasn't possible to look for higher modes in higher frequency regions. Also this dip is not visible in the simulation.

4.2.2 Remarks on the qubit without chargeline

Due to time reasons, no measurements were performed with the qubit closer than approximatetely 1 GHz from the resonator frequency. After a first measurement the results for T_1 looked very noisy around the lower sweetspot, so T_2^* and T_1 were measured again a second time for some of the frequencies to verify the validity of the resulting data. Most of the data points have similar values for T_1 and T_2^* for both measurements. But at the (lower) sweetspot frequency, the times of the second measurement have the double size of the ones from the first measurement. Since the Ramsey and T_1-Time-Measurement data of the first measurement do not fit the exponential decay very well at the (lower) sweetspot frequency, the measurement values are more reliable than the ones from the first measurement for the (lower) sweetspot frequency. Also in the plot of the dephasing T_2^* the two sweetspots are visible (for the qubit without chargline), where T_2^* increases ($\nu \sim$8.1 GHz & $\nu \sim$5.3 GHz).

4.3 Comparing the results with and without chargeline

As it can be seen in Figure 30, T_1 is very similar for the two qubits. So it seems that the chargeline doesn't affect the experimental T_1 very much.
Moreover, due to the lower sweetspot of the qubit without chargeline it was not possible to measure further down to check if there was a dip to for this qubit (the lower sweetspot lies exactly in the dip of the qubit with chargeline).
All in all, there are some frequencies that show more or less "good" T_1 or T_2^* times. The problem is, that most of the frequencies, which have "good" T_1, have a "bad" T_2^*. For example, at $\nu_{qubit} \approx 4.7$ GHz, there is a "good" T_1 of $\sim$ 10 500 ns and a bad T_2^* of $\sim$ 300 ns for the qubit with chargeline.

5 Discussion

In the previous sections all the results were presented and an interpretation of them was given. Now the most important points will be discussed.
It was mentioned that the difference in the "multimode model" could be explained with a constant offset in the bandwidth corresponding to internal losses. Again this is strange since all the metal was set lossless in Sonnet to cancel out resistive losses as a limiting factor. But on the other hand the output admittance matrix from Sonnet was not purely imaginary and was made imaginary by deleting the real part of it (as mentioned in 2.3). When these real parts, which were very small and looked like numerical errors, were first observed, two simulations were performed, one with the default admittance matrix with the small real parts and one where the real parts were all set to zero. The result of those simulations is visible in Figure 31.

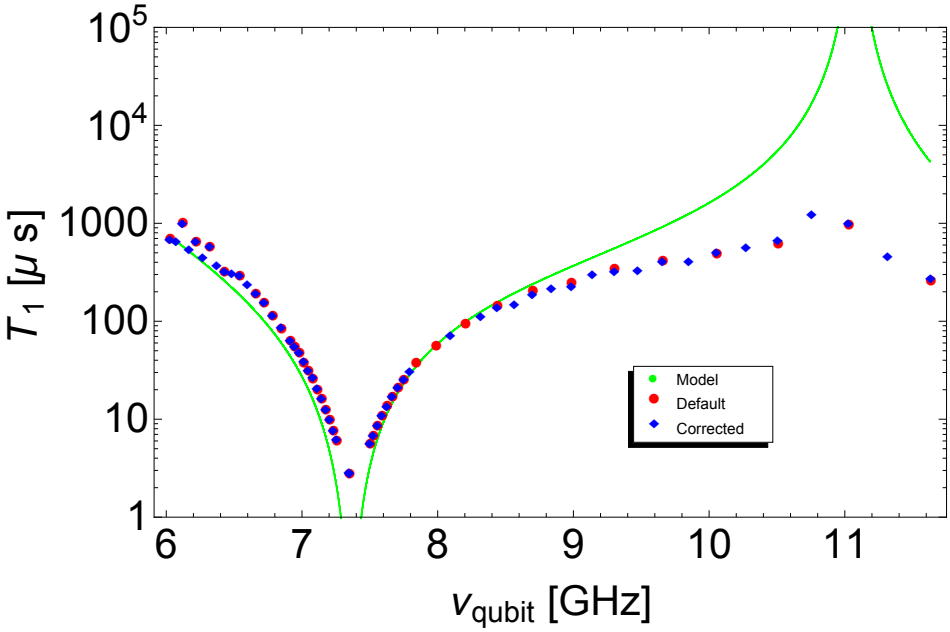

Figure 31: Combined results for T_1 for the **default** admittance matrix (which had non-zero real parts) and the **corrected** admittance matrix (with deleted real parts).

By comparing T_1 for the two kind of admittance matrices, there is no real difference visible. On one hand, this justifies deleting the real part to correct the admittance matrix to the form it should physically have. This correction was then done for all the other presented simulations in the thesis. On the other hand, it doesn't solve the questions were the losses are coming from. Nevertheless it can be a hint that there are unrealistic values in the output of Sonnet, which are hidden somewhere in the Sonnet output.
Coming from this point of view it would be interesting to do simulations with Maxwell as well and compare the results to those which were performed with Sonnet. This was done for one qubit (length 480 μm, width 80 μm, separation 35 μm and with chargeline).
The behavior of the resulting T_1 times, which were simulated with the capacitance matrix from Maxwell, is quite the same. Even though due to very narrow peaks data in the interesting off-resonant-region couldn't be properly gathered. But the problem of the difference between simulation and model is also present in the Maxwell simulation.
What is really interesting though, is that the resulting qubit-resonator-coupling g has almost half the value of the one from Sonnet ($g^{Max} = 52.6\,\text{MHz}$ and $g^{Son} = 117.4\,\text{MHz}$). So there appeared the questions: Why are they so different and which one is more reliable?

The value of g can be calculated theoretically with the capacitance matrix which in the past yielded results close to the experimental ones. Therefore the error was believed to be in a "default setting" in Sonnet. Hence the "default setting" for the co-calibrated ports were changed. In "Port Properties/Calibration Group/Properties...", the "Ground Node Connection" was changed from "Sonnet Box" to "Floating" and the "Terminal Width" was changed from "Feedline Width" to "One Cell". Afterwards another simulation for the mentioned geometry was performed with the alternative settings in Sonnet.
The results of the Maxwell simulation are plotted together with the results from the Sonnet simulation with the new and the old port settings in Figure 32. The resulting qubit-resonator-coupling for the alternative settings Sonnet simulation was $g^{SonAlt} = 48\,\mathrm{MHz}$ which is much closer to the one from Maxwell ($g^{Max} = 53\,\mathrm{MHz}$) compared to the Sonnet simulation with default settings ($g^{SonDef} = 117\,\mathrm{MHz}$).

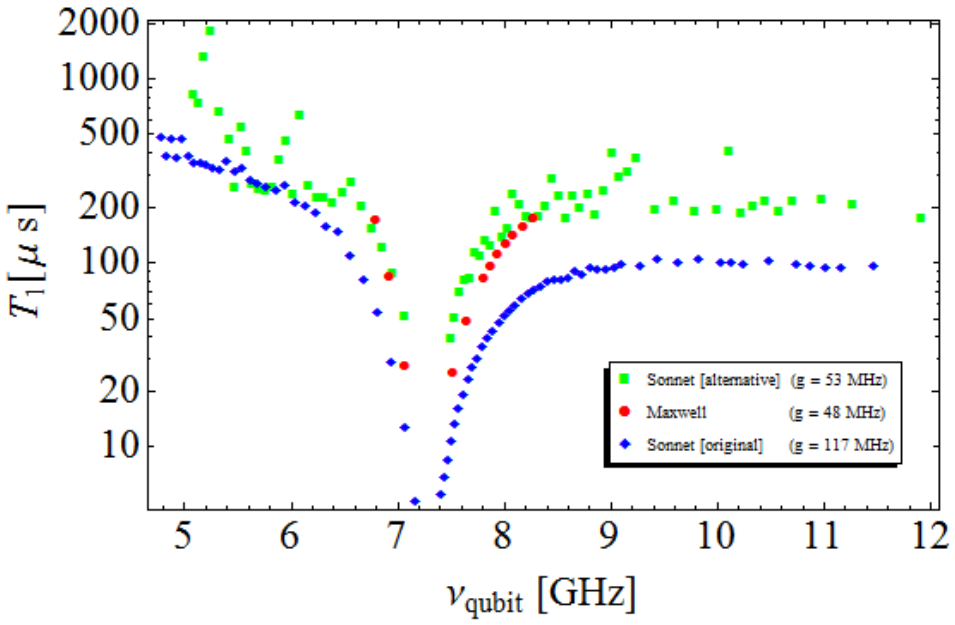

Figure 32: The resulting T_1 from the original (**default** settings) simulation with Sonnet, the simulation with Maxwell and the simulation with Sonnet with the **alternative** port setting.

Unfortunately, the alternative Sonnet simulation doesn't solve the problem with the losses since T_1 is also limited compared to the model. But it obviously solves the problem of the different outputs of Sonnet and Maxwell. Therefore there might be other setting of Sonnet which could lead to more realistic results.
Also it was mentioned that the resulting values for C_{eff} are much lower than expected. Now for the Maxwell simulation (C_{eff}^{Max}) and the "alternative" Sonnet simulation (C_{eff}^{ASon}) the values of C_{eff} for the simulated geometries are: C_{eff}^{Max}=57.14 fF and C_{eff}^{ASon}=53.67 fF. For this geometry the value of the "default" Sonnet simulation is C_{eff}^{DSon}=11.02 fF. A value for C_{eff} around 70 fF was expected from a crude dimensional analysis estimate, so the values of Maxwell and the "alternative" Sonnet simulation are much closer to this expected value compared to the "default" Sonnet simulation. This is also a hint that the Maxwell or "alternative port settings" Sonnet simulation are probably more realistic than the one with "default port settings" from Sonnet.
Since the Maxwell simulation was performed after all the other simulations were already finished, this default port setting was unfortunately used for all the other simulations with the "default settings" in Sonnet. Due to time reasons the simulations were not repeated with the "alternative

settings" in Sonnet. Also this problem in the "default port settings", is once more a sign that there might be settings somewhere in Sonnet, which are not completely understood for the type of simulations performed in this thesis and which cause the differences between simulation and model.
Moreover, it could be of course possible that the model should have some extra terms, which were not included but needed, to describe such an idealized system better. But then the question would be, how these terms should look like and what are the physical arguments to justify their integration into the model.
After the difference between simulation and model was outlined, the focus will be lied on the comparison between the simulation and the experimental results. In Figure 33 the resulting T_1 from the measurement are plotted logarithmically together with the data from the simulation for a qubit with and without chargeline. The data from the simulation is for a qubit with the same geometry parameter settings as the measured ones (length 480 μm, width 80 μm and separation 35 μm).

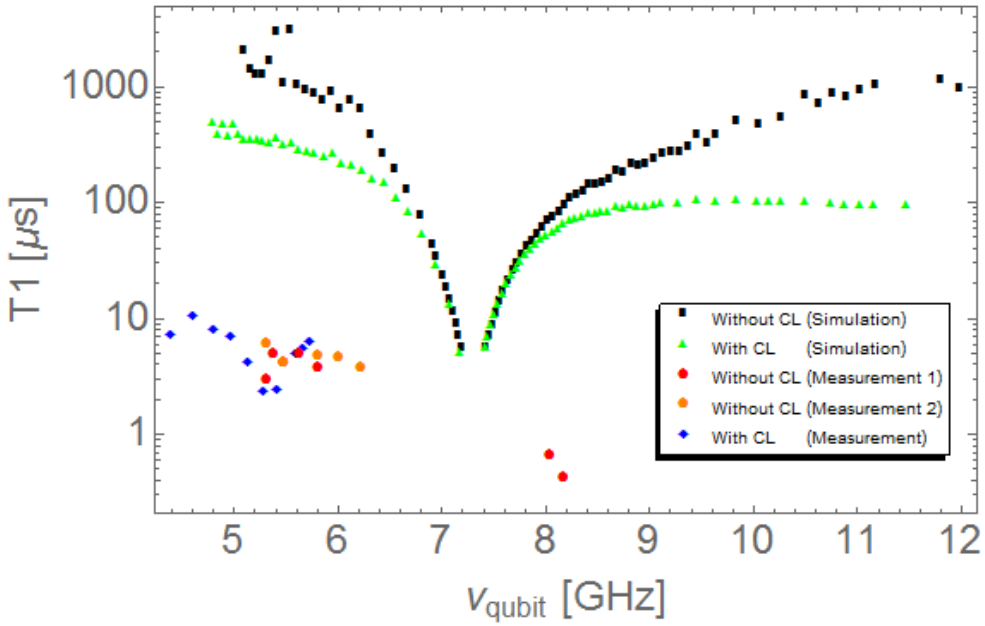

Figure 33: Experimental measured T_1 plotted logarithmically together with the simulated T_1 for the same geometry parameter settings and with & without chargeline.

The simulated T_1 are much bigger than the experimental T_1. This difference can not lie in the geometry and has to lie mostly in the experimental setup or the fabrication.
Such limiting factors arising from the experimental setup could be for example resonances between different parts of the measurement installation and the sample or thermal noise. There were different sweetspot frequencies for the two qubits, while the two qubits were designed to have the same sweetspot frequencies. Moreover, the qubit without chargeline had additionally an unexpected lower sweetspot. These factors are signs that the design which was on the blueprints could not be exactly mapped onto the real qubits, which is probably a consequence of the fabrication. So it might be that other limiting factors arise from the fabrication too.
Also the dip in T_1 for the qubit with chargeline wasn't visible in the simulation and therefore results from the setup or the fabrication.
Since the geometry parameters don't affect the simulated T_1 very much in the simulation it can be concluded that they are not the main limiting factors compared to setup and fabrication.

The chargeline affected the behavior of T_1 very much in the simulation and hence is a much bigger limiting factor in the simulation compared to the geometry. But in the measurement the chargeline has no strong direct effect on the experimental T_1 and is therefore probably also a very weak limiting factor compared to setup and fabrication.
Also the launcher was included in the Sonnet and Maxwell simulation and it could be that its position has an influence on T_1 due to its vicinity to the qubit.

6 Conclusion and Outlook

In conclusion, the simulated T_1 vary moderately for different geometries and change much for the chargeline. Additionally the behavior of the simulated data doesn't fully match the behavior expected from the analytical "multimode model". The difference can be reduced by introducing losses, whose origins lie somewhere in the used simulation programs and are unknown. Moreover, the measured T_1 are much lower than the simulated T_1, which is pointing towards much more significant limiting factors, caused by the fabrication and measurement setup, compared to the ideal values theoretically possible for the design.

In the following an outlook for possible improvements in the future is given. The problem of the somehow limited T_1 stays, so one further task would be to find those lossy effects in the Sonnet settings.
Moreover, the simulations that were performed with the "default port settings" could be repeated with the "alternative port setting" and/or with Maxwell.
For more efficient Maxwell simulations, it would be useful to enter (over a Python script) the capacitance matrix into the capacitance network in Microwave Office automatically.
The island length wasn't changed as a geometry parameter, hence the island length could be swept too.
As mentioned in the discussion, the position of the launcher could affect T_1 through some direct coupling between launcher an qubit. This could be checked by simulating T_1 for different position of the launcher in the blueprints.
And last but not least, the duration of the analysis program was around a few hours, so it would be nice to speed up the simulation procedure. The analysis program needs much time for the "nonlinear model fit" of Mathematica, therefore it would be good if this fitting time could be improved.

7 Appendix

7.1 Derivation of the multimode model bandwidth

The qubit can be approximated as LC-circuit sitting in a capacitive box (capacitance network) which is connected to other elements with impedance Z and input voltage V_{in} visible in Figure 34(a). The impedance has a real part $Re(Z) = R$, which can be interpreted as a source of Johnson-Nyquist noise. The capacitance network represented by the blue box, visible in Figure 34(a), acts as of a capacitive voltage divider. This means that the input voltage V_{in} is transformed to some effective voltage seen by the qubit, which is proportional to V_{in}. Therefore the voltage applied to the "qubit system" can be written as $\tilde{V} = \beta V_{in}$.
We can model the noisy resistor as an ideal resistor combined with a noisy part as illustrated in Figure 34(b). The squared standard deviation of the voltage of the noisy part is then proportional to the real resistance, hence $\sigma^2_{V_{in}} \approx R$. Since the voltage seen by the "qubit system" is given as $\tilde{V} = \beta V_{in}$ its standard deviation will satisfy $\sigma_{\tilde{V}} = \beta \sigma_{Vin}$. Therefore we can write $\sigma^2_{\tilde{V}} = \sigma^2_{Vin}\beta^2 \approx R\beta^2$. Additionally we can represent the voltage noise (with a standard deviation of $\sigma^2_{\tilde{V}}$) by a resistor with a resistance of $R\beta^2$. By using this, the system, visible in Figure 34(a), can be mapped onto the system which is depicted in Figure 34(c).

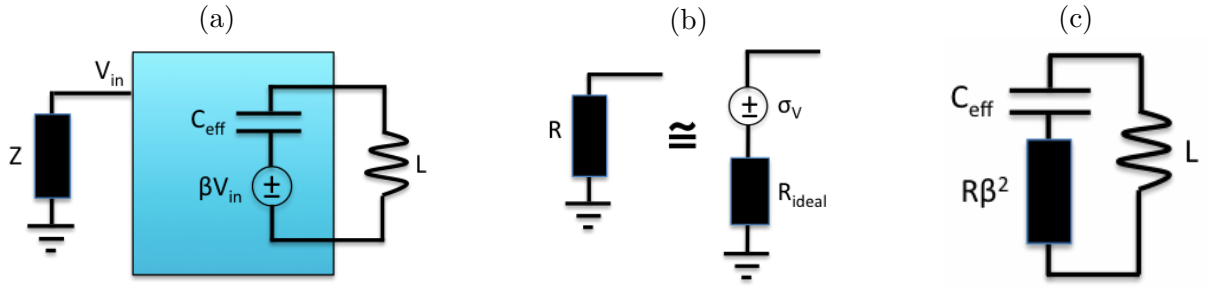

Figure 34: (a)A schematic drawing of the on-chip-elements. (b) Approximation of a real noisy resistor and an ideal resistor plus a noisy source. (c) The resulting schematic of the approximative mapping explained in the text.

Now by applying Kirchhoff's law, the relation $i\omega L + 1/(i\omega C_{eff}) + R\beta^2 = 0$ can be obtained. This is a quadratic equation in ω which has the solutions

$$\omega_{\pm} = -\frac{R\beta^2 \pm \sqrt{R^2\beta^4 - 4\frac{L}{C_{eff}}}}{2iL} = i\frac{R\beta^2}{2L} \pm \sqrt{\frac{1}{LC_{eff}} - (\frac{R\beta^2}{2L})^2}\ .$$

This can be equated to $\omega_{\pm} = i\frac{\Gamma}{2} \pm \tilde{\omega}$, while we have defined

$$\Gamma = \frac{R\beta^2}{L} \tag{4}$$

It is known that the dynamics of such a system (I and V) can be written as superposition of the two eigenfrequencies in the following way

$$I(t) = Ae^{i\omega_+ t} + Be^{i\omega_- t} = e^{-\frac{\Gamma}{2}t}\left[Ae^{i\tilde{\omega}t} + BAe^{-i\tilde{\omega}t}\right]$$

Therefore the energy E $\propto I^2 \propto e^{-\Gamma t}$ is damped with the damping constant Γ and hence this Γ can be interpreted as the inverse of the relaxation time T_1.

By using the relation for the capacitance energy of the Josephson junction $E_C = \frac{e^2}{2C_{eff}}$ (C_{eff}

is the effective capacitance of the qubit), together with the relation for the frequency of an LC-oscillator $\omega = \frac{1}{\sqrt{LC_{eff}}}$, this can be written as

$$\Gamma = \frac{\omega^2 e^2 \beta^2 Z_0}{2E_C} \frac{R}{Z_0}. \tag{5}$$

In the following, we derive a formula for the effective resonator capacitance C_0.
On one hand, the electrical energy of the transmissionline-resonator can be written as averaged value over the capacitance per length $\frac{\Delta C}{\Delta l}$ times the voltage $V^2(x)$ along the resonator

$$E_{el} = \frac{1}{2} \int_0^l \frac{\Delta C}{\Delta l} [V(x)]^2 dx$$

with l the length of the resonator and the oscillating voltage $V(x) = V cos(kx)$ inside the resonator. We substitute $\varphi = kx = \frac{2\pi x}{l}$ and integrate

$$E_{el} = \frac{1}{2} \frac{\Delta C}{\Delta l} V^2 \frac{l}{2\pi} \int_0^{2\pi} \cos^2(\varphi) d\varphi = \frac{1}{2} \Big[\frac{1}{2} \frac{\Delta C}{\Delta l} l \Big] V^2$$

On the other hand, we can write the electrical energy with the effective capacitance as $E_{el} = \frac{1}{2} C_0 V^2$. By comparing both terms we obtain

$$C_0 = \frac{1}{2} \frac{\Delta C}{\Delta l} l \tag{6}$$

Now we use the general relations for the impedance

$$Z_0 = \sqrt{\frac{\Delta L}{\Delta C}} = \sqrt{\frac{\Delta L / \Delta l}{\Delta C / \Delta l}}$$

and for the velocity of the signal

$$v = \frac{\Delta l}{\sqrt{\Delta L \Delta C}} = \frac{1}{\sqrt{\Delta L / \Delta l \cdot \Delta C / \Delta l}}$$

which we can combine to $\Delta C / \Delta l = 1/(Z_0 v)$. Next we use that for this transmission line which is open at one end, the phase has to satisfy $\pi = \phi = \frac{\omega_0 l}{v}$, so by using equation (6) we end up with

$$C_0 = \frac{1}{2} \frac{\Delta C}{\Delta l} l = \frac{1}{2} \frac{l}{Z_0 v} = \frac{\pi}{2 Z_0 \omega_0} \tag{7}$$

To continue, we first need a few relations from paper [3]:

$$\hbar g_{ij} = 2\beta e V^0_{rms} \langle i | \hat{n} | j \rangle \tag{8}$$

$$\langle m+1 | \hat{n} | m \rangle \approx \sqrt{\frac{m+1}{2}} \Big(\frac{E_J}{8E_C} \Big)^{1/4} \tag{9}$$

$$\hbar \omega \approx \sqrt{8 E_C E_J} \tag{10}$$

$$V^0_{rms} = \sqrt{\hbar \omega_0 / 2C_0} \tag{11}$$

They are equations (3.3),(3.4) and (2.11) in paper [3], while we approximated relation (2.11) and β as the same quantity we used in the derivation above. Our equation (11) is written in the text between (3.1) and (3.2) in this paper and we set $C_r = C_0 \,\&\, \omega_r = \omega_0$.
Because we are just looking at the transition $i = 1 \,\&\, j = 0$ equation (8), (9) and (11) can be combined to

$$g = g_{10} = \frac{2\beta e}{\hbar}\sqrt{\frac{\hbar\omega_0}{2C_0}}\,\langle 1|\hat{n}|0\rangle \approx \frac{2\beta e}{\hbar}\sqrt{\frac{\hbar\omega_0}{2C_0}}\sqrt{\frac{1}{2}}\Big(\frac{E_J}{8E_C}\Big)^{1/4}$$

of which we square both sides

$$g^2 \approx \frac{4\beta^2 e^2}{\hbar^2}\frac{\hbar\omega_0}{2C_0}\frac{1}{2}\frac{1}{8E_C}\sqrt{8E_C E_J} = \frac{4\beta^2 e^2}{\hbar}\frac{\omega_0}{2C_0}\frac{1}{2}\frac{1}{8E_C}\hbar\omega = \frac{\beta^2 e^2\omega_0}{4E_C}\frac{2Z_0\omega_0}{\pi}\omega$$

while we used equation 7. Now this can be rearranged to

$$\frac{2g^2\pi\omega}{\omega_0^2} \approx \frac{\omega^2 e^2\beta^2 Z_0}{2E_C} \tag{12}$$

Relation (12) can be plugged into equation (5) to obtain

$$\Gamma = \frac{2g^2\pi\omega}{\omega_0^2}\frac{R}{Z_0}. \tag{13}$$

We proceed with the last part of our derivation by finding another expression for R.
The resistance R is given by the real part of the total impedance of the elements of the circuit without the qubit. In Figure 35 the different elements are depicted.

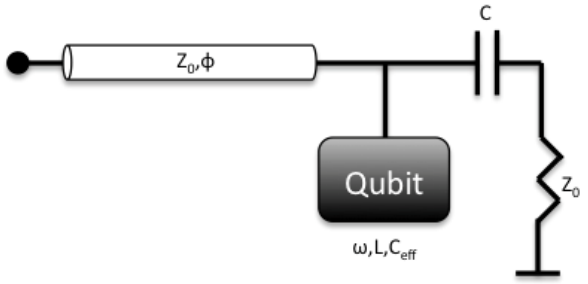

Figure 35: Schematic drawing of the on-chip circuit with qubit, transmission-line-resonator, capacitive coupling and impedance.

So the total impedance of all the elements but the qubit is then

$$\begin{aligned} Z &= \frac{1}{\frac{i\tan(\phi)}{Z_0} + \frac{1}{Z_0 + \frac{1}{i\omega C}}} = \frac{1}{i\Big(\frac{\tan(\phi)}{Z_0} + \frac{\omega C}{1 + i\omega C Z_0}\Big)} \\ &= \frac{1 + i\omega C Z_0}{i\big(\omega C + Z_0^{-1}\tan(\phi) + i\omega C\tan(\phi)\big)} \\ &= -i\frac{\big(1 + i\omega C Z_0\big)\big(\omega C + Z_0^{-1}\tan(\phi) - i\omega C\tan(\phi)\big)}{\big(\omega C + Z_0^{-1}\tan(\phi)\big)^2 + \big(\omega C\tan(\phi)\big)^2} \end{aligned}$$

we take the real part of Z and divide by Z_0

$$\begin{aligned}
\frac{Re(Z)}{Z_0} &= \frac{1}{Z_0} Re\Big(-i \frac{\omega C + \omega^2 C^2 Z_0 \tan(\phi) + i\omega^2 C^2 Z_0}{\big(\omega C + Z_0^{-1}\tan(\phi)\big)^2 + \big(\omega C \tan(\phi)\big)^2)} \Big) \\
&= \frac{\omega^2 C^2 Z_0^2}{\big(\omega C Z_0 + \tan(\phi)\big)^2 + \big(\omega C Z_0 \tan(\phi)\big)^2} \\
&= \frac{\big(\omega C Z_0\big)^2}{(\omega C Z_0)^2 + \tan^2(\phi) + 2\omega C Z_0 \tan(\phi) + \big(\omega C Z_0\big)^2 \tan^2(\phi)} \\
&= \frac{\big(\omega C Z_0\big)^2 \cos^2(\phi)}{\big(\omega C Z_0\big)^2 \big(\cos^2(\phi) + \sin^2(\phi)\big) + \sin^2(\phi) + 2\sin(\phi)\cos(\phi)\omega C Z_0} \\
&= \frac{\big(\omega C Z_0\big)^2 \cos^2(\phi)}{\big(\omega C Z_0\big)^2 + \sin^2(\phi) + \sin(2\phi)\omega C Z_0}
\end{aligned}$$

So in the end, by inserting $\frac{R}{Z_0} = \frac{ReZ}{Z_0}$ into equation (13), we end up with

$$\underline{\underline{\Gamma = \frac{2g^2\pi\omega}{\omega_0^2} \frac{\big(\omega C Z_0\big)^2 \cos^2(\phi)}{\sin^2(\phi) + \omega C Z_0 \sin(2\phi) + \big(\omega C Z_0\big)^2}}}$$

It is to mention, that we also used a trick to substitute CZ_0 in the model through a quantity that could be determined through the simulation. For this we look at the general relation for an asymmetric double sided resonator

$$\omega + i\frac{\kappa}{2} = \omega_0(1 - \lambda + \lambda^2 + in\pi\lambda^2)$$

while λ is given by

$$\lambda = CZ_0 \frac{v}{l}$$

with l the length of the resonator and v velocity of the signal in the resonator. With the relation for the fundamental mode of the resonator frequency $\omega_0 = \pi v/l$ we can compare real and imaginary part in the first relation and obtain (again n=1)

$$\kappa = \frac{2C^2 Z_0^2 \omega_0^2}{\pi} \Rightarrow CZ_0 = \sqrt{\frac{\kappa\pi}{2\omega_0^3}} \ .$$

By using that $\kappa = 2(2\pi\bar{\Gamma}_{resonator})$ with the on-resonant bandwidth $\bar{\Gamma}_{resonator}$. This can be approximated for our simulation as $\kappa \approx 4\pi min(\Gamma_{resonator})$ since the bandwidth of the resonator has the lowest values in the on-resonant region. So this finally gives us the expression

$$\underline{CZ_0 \approx \sqrt{\frac{2\pi^2 min(\Gamma_{resonator})}{\omega_0^3}}}$$

which we have plugged into the "model equation" (3) for the plots in the Figures which contain the data of the model.

7.2 Fit functions for g and C_{eff}

First, the fit function for g will be derived. We start with the eigenenergies of the Jaynes-Cummings Hamiltonian given by [1]

$$\frac{E_n^{\pm}}{\hbar} = \omega_0 n \pm \frac{1}{2}\sqrt{(\omega-\omega_0)^2 + 4g^2 n}$$

with "+" for the excited, "−" for the ground state, n the photon number, ω & ω_0 the tuned frequencies of the qubit and the resonator and g the qubit-resonator-coupling in GHz. Now let us consider n=1 and take the frequency difference $\frac{E^+}{h} - \frac{E^-}{h} = \Delta$

$$\Delta = \sqrt{\Big(\frac{\omega}{2\pi} - \frac{\omega_0}{2\pi}\Big)^2 + \Big(\frac{g}{\pi}\Big)^2} = \sqrt{\big(\nu-\nu_0\big)^2 + \Big(\frac{g}{\pi}\Big)^2}.$$

By approximating the qubit and resonator as LC-oscillators for our simulation setup, we can approximate ν & ν_0 as

$$\nu = \frac{\omega}{2\pi} \approx \frac{1}{2\pi\sqrt{LC_{eff}}} = \sqrt{\frac{\alpha}{L}}$$
$$\nu_0 = \frac{\omega_0}{2\pi} \approx \frac{1}{2\pi\sqrt{L_{res}C_0}} = \sqrt{\frac{\alpha}{L_0}}$$

with their corresponding inductive tunings L and $L_0 = L_{res}\frac{C_0}{C_{eff}}$ and the definition $\alpha = \frac{1}{4\pi^2 C_{eff}}$. By plugging this into the equation above we finally obtain

$$\underline{\Delta = \sqrt{\alpha\Big(\frac{1}{\sqrt{L}} - \frac{1}{\sqrt{L_0}}\Big)^2 + \Big(\frac{g}{\pi}\Big)^2}}$$

Second, we look at the fit function for C_{eff}. Again we approximate the qubit as an LC-oscillator and use $\omega = 2\pi\nu$ to get

$$2\pi\nu_{qubit} = \omega_{qubit} = \frac{1}{\sqrt{LC_{eff}}} \quad \Rightarrow \quad \underline{\nu_{qubit} = \frac{1}{2\pi\sqrt{LC_{eff}}}}$$

References

[1] M. Baur, Ph.D. thesis, ETH Zurich, *Realizing quantum gates and algorithms with three superconducting qubits*, 2012.

[2] A.A. Houck et al., *Controlling the Spontaneous Emission of s Superconducting Transmon Qubit*, Physical Review Letters 101.080502 (2008).

[3] J. Koch et al., *Charge insensitive qubit design derived from the Cooper pair box*, Phys. Rev. A 76, 042319 (2007).

[4] Maxwell, Version 14.0,
http://www.ansys.com/Products/Simulation+Technology/
Electronics/Electromechanical/ANSYS+Maxwell

[5] Microwave Office (AWR Design Environment 11),
http://www.awrcorp.com/products/microwave-office

[6] Sonnet, Version 15.52,
http://www.sonnetsoftware.com

[7] Source for connection between Python and Microwave Office,
https://awrcorp.com/download/faq/english/scripts/
script_in_python_and_perl.aspx

ETH

Eidgenössische Technische Hochschule Zürich
Swiss Federal Institute of Technology Zurich

Eigenständigkeitserklärung

Die unterzeichnete Eigenständigkeitserklärung ist Bestandteil jeder während des Studiums verfassten Semester-, Bachelor- und Master-Arbeit oder anderen Abschlussarbeit (auch der jeweils elektronischen Version).

Die Dozentinnen und Dozenten können auch für andere bei ihnen verfasste schriftliche Arbeiten eine Eigenständigkeitserklärung verlangen.

Ich bestätige, die vorliegende Arbeit selbständig und in eigenen Worten verfasst zu haben. Davon ausgenommen sind sprachliche und inhaltliche Korrekturvorschläge durch die Betreuer und Betreuerinnen der Arbeit.

Titel der Arbeit (in Druckschrift):

Simulating qubit relaxation times to analyze limiting factors of the electromagnetic environment

Verfasst von (in Druckschrift):
Bei Gruppenarbeiten sind die Namen aller Verfasserinnen und Verfasser erforderlich.

Name(n):	**Vorname(n):**
Allenspach	Stephan

Ich bestätige mit meiner Unterschrift:
- Ich habe keine im Merkblatt „Zitier-Knigge" beschriebene Form des Plagiats begangen.
- Ich habe alle Methoden, Daten und Arbeitsabläufe wahrheitsgetreu dokumentiert.
- Ich habe keine Daten manipuliert.
- Ich habe alle Personen erwähnt, welche die Arbeit wesentlich unterstützt haben.

Ich nehme zur Kenntnis, dass die Arbeit mit elektronischen Hilfsmitteln auf Plagiate überprüft werden kann.

Ort, Datum	**Unterschrift(en)**
Zürich, 20.09.2015	Stephan Allenspach

Bei Gruppenarbeiten sind die Namen aller Verfasserinnen und Verfasser erforderlich. Durch die Unterschriften bürgen sie gemeinsam für den gesamten Inhalt dieser schriftlichen Arbeit.